The relationship between *BRAF* genetic alterations and the risk of tumour recurrence in Pilocytic Astrocytomas in children diagnosed at Red Cross Children's Hospital over a 33-year period.

MMed student: Dr Nandi Viljoen

Student number: GRCNAN001

Principal Investigator: Professor Komala Pillay

Division of Anatomical Pathology, University of Cape Town/Red Cross Children's Hospital

Co-investigators: Dr Amsha Ramburan

Division of Anatomical Pathology, University of Cape Town

Dr Shivani Singh

Division of Anatomical Pathology, University of Cape Town

Dr Nadia Ikumi

Division of Anatomical Pathology, University of Cape Town

Thesis submitted in partial fulfilment of the requirements for the degree MMed (Anatomical Pathology) in the Department of Anatomical Pathology, Faculty of Health Sciences, University of Cape Town.

Declaration

I, Dr Nandi Viljoen, hereby declare that the work on which this dissertation is based is on my original work (except where acknowledgements indicate otherwise) and that neither the whole work nor any part of it has been, is being, or is to be submitted for another degree in this or any other university.

I empower the university to reproduce for the purpose of research either the whole or any portion of the contents in any manner whatsoever.

Signature: Signed by candidate

Date: 11/07/2023

Acknowledgements

I want to express my gratitude for all the help, advice, and encouragement from my supervisor and co-investigators, Professor Komala Pillay, Dr Amsha Ramburan, Dr Shivani Singh and Dr Nadia Ikumi.

The following individuals are also deserving of appreciation for their contributions to this MMed project:

- Raymond Kriel from the Department of Anatomical Pathology for all his hard work performing the laboratory-based tests.
- Dr Fortuna Bagula for sourcing literature for this study.
- The laboratory staff at Red Cross Children's Hospital for allowing me to access the histopathology records and results.

Table of Contents

Chapter 2: Materials and Methods

2.1. Ethics approval

2.2. Study Design and cohort selection

2.3. Immunohistochemistry

2.4. Fluorescence in situ hybridisation

2.5. RNA extraction

2.6. Spectrophotometry

2.7. cDNA synthesis

2.8. Polymerase chain reaction

2.9. Agarose gel electrophoresis

2.10. Statistical analysis

Chapter 3: Results

Chapter 4: Discussion

Chapter 5: Conclusion and Recommendations

References

Appendices

Appendix 1: Ethics approval

Appendix 2: Preparation of reagents

Appendix 3: Composite table of data captured and generated during this study

Appendix 4: Quantity and purity of each case from which RNA was extracted

Abstract:

Introduction:

Pilocytic astrocytomas (PAs), glial-derived neoplasms, are the most common central nervous system (CNS) tumours reported in the paediatric population. [1] PAs are circumscribed astrocytic gliomas associated with a favourable overall survival and thus regarded as low grade by the World Health Organisation (WHO), with a reported five-year survival rate between 75% to 100%. [2,3] Optimal treatment of partially resected, deep anatomic location and recurrent tumours are challenging. Over the past decades, PAs have been the object of an increasing number of molecular studies which tried to identify favourable and unfavourable prognostic factors. Essentially all PAs harbour genetic aberrations resulting in the deregulation of the MAPK signalling pathway, with *BRAF* gene mutations being the most frequent. [4] However, reports on the impact of specific mutations on patient prognosis are controversial. [5–8] Advances in molecular techniques have opened the door for further studies to determine the relationship between these *BRAF* alterations (point mutations and gene fusions) and the risk of tumour recurrence.

Purpose:

The overall aim of this study was to determine if *BRAF* genetic alterations impact patient prognosis. This was done by evaluating the expression of *BRAF* using immunohistochemistry (IHC), fluorescence-in-situ hybridisation (FISH) and polymerase chain reaction (PCR) and comparing it to tumour recurrence. The results will also be compared to clinicopathological findings.

Methods:

Study design:

A retrospective cohort laboratory-based study included all cases diagnosed with PAs that presented to Red Cross Children's Hospital (RCC) from January 1984 to December 2016.

Patient selection and data collection:

Convenient sampling was done by searching the electronic laboratory information database (Disa and NHLS TrakCare) of the Division of Anatomical Pathology for all cases diagnosed with PAs. Data collection included: age at diagnosis, tumour site, management and recurrence.

Laboratory methods:

Archived stained slides of all the cases were reviewed, the diagnosis was confirmed on histology, and tissue blocks were retrieved. The presence of *BRAF* genetic aberrations were examined using immunohistochemistry, FISH and PCR.

Results:

Sixty-nine paediatric patients with PAs were identified over the study period with a median age of 6 years. This included 33 females and 21 males (in 15 cases the gender was not documented). Most tumours (62.32%) were located in the cerebellum, followed by the cerebral hemisphere (18.84%). The tumour recurred in 21 individuals, of which 3 had incomplete surgical resections. 46.16% of supratentorial tumours recurred compared to a recurrence risk of only 20.93% in infratentorial tumours. *BRAF* immunohistochemistry was negative in all the cases, and FISH studies did not show *BRAF* rearrangements.

Conclusion:

The findings of this study were broadly consistent with published literature in terms of age at presentation, location of the tumour and tumour location concerning the risk of recurrence. While most studies revealed an equal or slight male predominance, this study showed that the tumour developed slightly more frequently in females. Our study did not find a correlation between the risk of recurrence and *BRAF* genetic aberrations.

List of abbreviations

PA	Pilocytic Astrocytoma
CNS	Central Nervous System
WHO	World Health Organisation
IHC	Immunohistochemistry
FISH	Fluorescence-in-situ Hybridisation
PCR	Polymerase Chain Reaction
RCC	Red Cross Children's Hospital
GAP	GTPase- activating Protein
NF	Neurofibromatosis
BRAF	V-Raf murine sarcoma viral oncogene homolog B1
RAS	Rat sarcoma
MAPK	Mitogen-activated Protein Kinase
CT	Computed Tomography
MRI	Magnetic Resonance Imaging
FLAIR	Fluid-attenuated Inversion Recovery
H&E	Haematoxylin and Eosin
PMA	Pilomyxoid Astrocytoma
GFAP	Glial Fibrillary Acidic Protein
OLIG2	Oligodendrocyte Lineage Transcription Factor 2
IDH1	Isocitrate Dehydrogenase 1
RTK	Receptor Tyrosine Kinase
GDP	Guanosine Diphosphate
GTP	Guanosine Triphosphate
AP1	Activator Protein 1
GPCR	G-protein Coupled Receptor
FGFR1	Fibroblast Growth Factor Receptor 1
KRAS	Ki-ras2 Kirsten rat sarcoma viral oncogene homolog
NTRK	Neurotropic Tropomyosin Receptor Kinase
WT	Wild Type
Mut	Mutation
CSR	Complete Surgical Resection
FFPE	Formalin-fixed Paraffin-embedded
dNTP	Deoxynucleoside Triphosphate

List of Figures

List of Tables

List of Appendices

Chapter 1

Introduction and Literature Review

1.1. Background, epidemiology and clinical presentation:

Malignant neoplasms are the second most common cause of paediatric deaths worldwide. A 1% annual increase in newly diagnosed paediatric neoplasms occurred from 1997 to 2018. [9] Pilocytic astrocytomas (PAs) make up 19.7% of all brain cancers. [1] With 75% of cases recorded before age 20, there is evidence of an age-related decline in incidence. [10] Despite the gender distribution being typically equal, specific reports have revealed a slight male predominance. [11]

PAs are circumscribed astrocytic gliomas associated with a favourable overall survival and thus regarded as low grade by the World Health Organisation (WHO), with a reported five-year survival rate between 75% to 100%. [2,3] These tumours are characteristically curable by complete surgical resection. However, some tumours may be anatomically inoperable, and complete surgical resection is impossible.

Even though PAs can form anywhere along the neuroaxis, they seem to prefer the posterior fossa, where 65% of cases have been documented in the cerebellum. [1,12] The optic chiasm, hypothalamus, brain stem, and spinal cord are additional frequent sites. [13] Although these neoplasms are rare in adults, Burkhard et al. reported a higher chance of cerebral hemispheric presentation with advancing patient age. [2]

The clinical symptoms are usually insidious and depend on the localisation of the tumour. More noticeable neurological abnormalities will result from tumours occurring in specific functional areas of the brain compared to other locations presenting with more subtle changes. [14] Headaches are frequently the primary symptom of tumours developing in the posterior fossa, and other complaints include nausea, vomiting, neck stiffness, blurred vision and dizziness. Tumours in this region can also lead to cerebellar and cranial nerve dysfunction manifesting as gait disturbances, cranial nerve palsies, and bulbar dysfunction. [15,16] Visual field deficit, visual loss or proptosis, is the complaint when the tumour compresses the optic chiasm. Hypothalamic/pituitary dysfunction, for instance, diabetic insipidus, is seen when the tumour arises in the hypothalamus. Primary spinal cord tumours often result in back pain, while larger more advanced lesion can result in loss of sensation, muscle weakness and urinary incontinence, amongst others. Primary tumours in brain regions necessary for

processing auditory information, personality expression, and short-term memory frequently have less obvious clinical symptoms, which might delay detection. [14] Multicentric and diffuse leptomeningeal dissemination is extremely rare.

1.1.1. Pilocytic astrocytoma and syndromic associations:

The majority of PAs occur sporadically, however, a small percentage has been reported in some neurodevelopmental diseases. These include neurofibromatosis type 1 syndrome, Noonan syndrome, encephalocraniocutaneous lipomatosis and Noonan syndrome with multiple lentigines (NSML), which was formerly known as LEOPARD syndrome. [17–19]

The most prevalent of them is neurofibromatosis type 1 (NF1) syndrome. [20] 1 in 4000 people have the genetically inherited autosomal dominant condition NF1 syndrome. [21] Abnormal function of the *NF1* gene leads to uncontrolled growth resulting in tumour development. *NF1* gene encodes the tumour suppressor protein neurofibromin which acts as a GTPase-activating protein (GAP) for Rat sarcoma (Ras) protein. Mutational neurofibromin causes uncontrolled activation of the MAPK molecular pathway. [22] Two or more clinical signs must be present to diagnose NF1 syndrome. These can include a combination of Lisch nodules, specific skin abnormalities, optic pathway glioma/PA or multiple neurofibromas. [23] The optic pathway is frequently affected by PAs observed in this setting, and they have reported higher survival rates. [20]

Noonan syndrome is a genetically inherited disorder with a reported incidence of 1 per 1500 to 2500 people. [24] The clinical manifestations are varied, including abnormal facial features, congenital heart defects, short stature, and hearing and learning deficits. According to reports, up to 50% of cases involve abnormalities in the *PTPN11* gene. [24] Genetic alterations involving different components along the MAPK/RAS signalling cascade are seen in the remainder of the issues.

1.2. Diagnosis:

1.2.1. Imaging modalities:

Computed tomography (CT) and magnetic resonance imaging (MRI) are the neuroradiological imaging techniques that can be used to diagnose PAs. CT scans are often the first modality performed in children presenting with symptoms. However, CT scans; even with contrast administration; are often insufficient for adequate visualisation of specific tumour characteristics. It also carries a risk for secondary radiation-induced cancers. [25] The ideal

technique to confirm the diagnosis is MRI, although it is more costly and time-consuming compared to CT.

The imaging features of PAs can be variable in both CT and MRI. However, the most consistent finding in up to two-thirds of tumours is a well-circumscribed cystic lesion with a smooth border and a solid mural nodule. On CT, the solid mural nodule is often hypo- or isointense and contrast-enhancing. Whilst using MRI, the solid areas will display T2 hyperintensity (Figure 1.1B) and T1 hypointensity (Figure 1.1A). [26] The tumour can also display small areas of calcification on CT imaging. [27] The adjacent brain is normal and rarely displays minimal peritumoral oedema, a reassuring feature since this is often associated with high-grade gliomas.

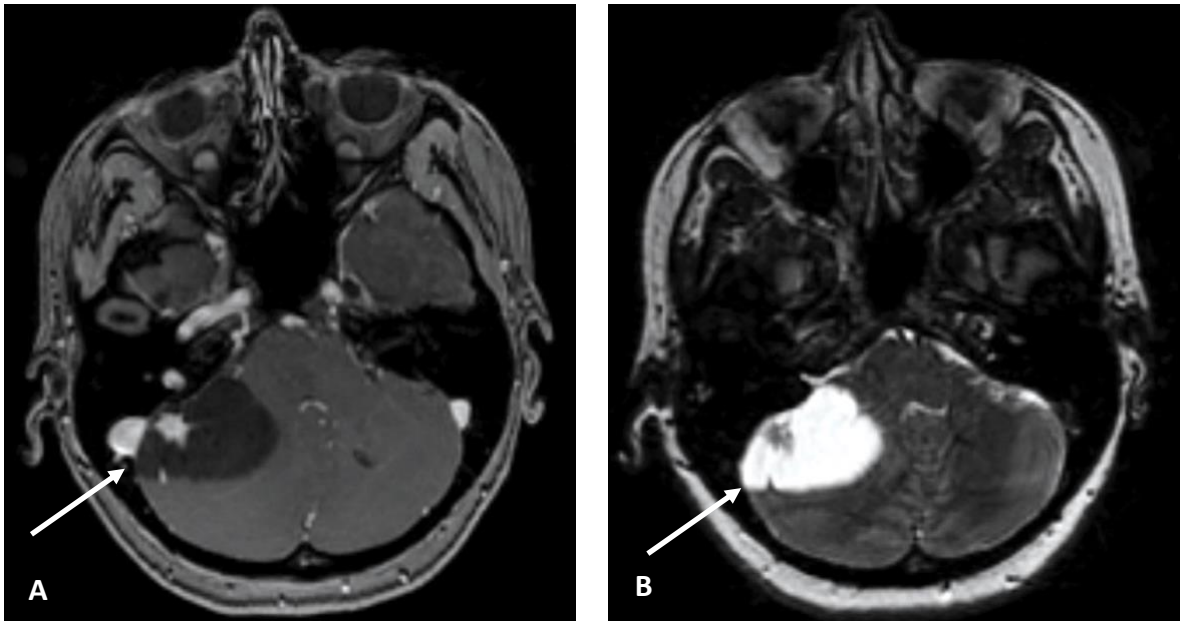

Figure 1.1: A: Contrast-enhanced T1 weighted MRI of a PA showing the characteristic solid-cystic tumour with a diffusely enhancing solid component. [23] **B: T2-weighted MRI image displaying hyperintensity of the solid regions.**[23]

The radiological differential diagnosis for children presenting with cerebellar, circumscribed, solid-cystic lesions include PAs, ganglioglioma, pleomorphic xanthoastrocytoma, and haemangioblastoma. A definite diagnosis is made on biopsy for histopathological assessment.

1.2.2. Histopathological diagnosis:

Macroscopic examination of PAs reveal a soft cystic mass with a firm mural nodule that can have foci of calcification. [17] The cyst fluid is often brown and proteinaceous. Spinal tumours

can be associated with syrinx formation. [28] Encasement of the optic sheath is often seen in tumours in the optic chiasm. [29]

On histological assessment, PAs show low to moderate cellularity with a sharp interface to the adjacent unaffected brain. Rarely, tumours may invade the nearby brain, mimicking higher-grade tumours. However, the overall microscopic findings of PAs are diagnostic due to their biphasic nature comprising compact piloid zones adjacent to loosely textured microcystic areas (Figure 1.2). The compact regions are rich in astrocytic cells with elongated nuclei, bipolar fibrillary processes and Rosenthal fibres. Rosenthal fibres (Figure 1.3) are elongated, brightly eosinophilic corkscrew-shaped intracytoplasmic inclusions measuring 10 – 40 µm in diameter and appear as electron-dense bodies on electron microscopy. [30–32] These fibres can be viewed as reactive changes in the unaffected brain adjacent to other low-grade tumours, around cysts, and in metabolic illnesses like Alexander's disease. They are not pathognomonic for PAs.

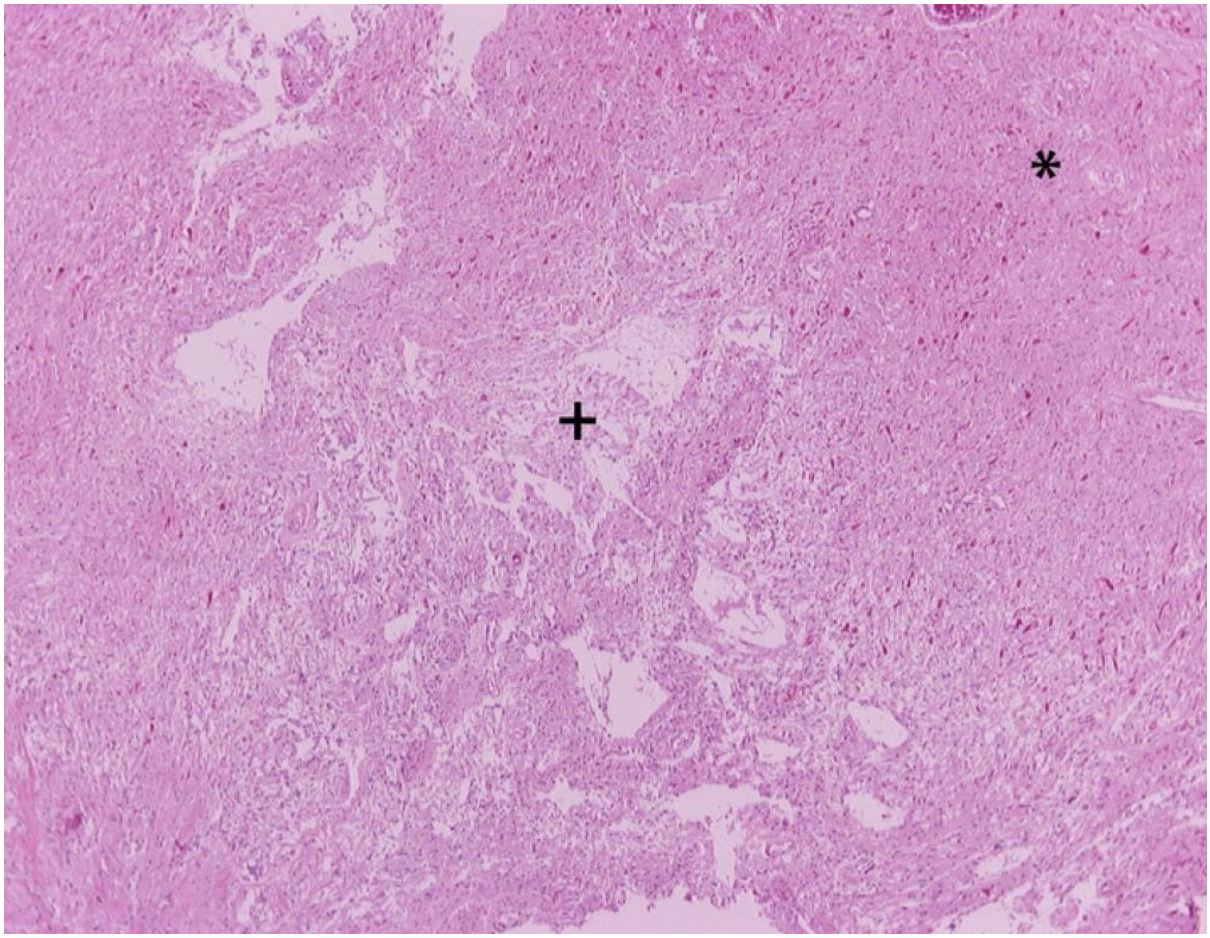

Figure 1.2: Haematoxylin and eosin stain of a pilocytic astrocytoma displaying biphasic compact (*) and looser, microcystic (+) areas (H&E, 40x). [33]

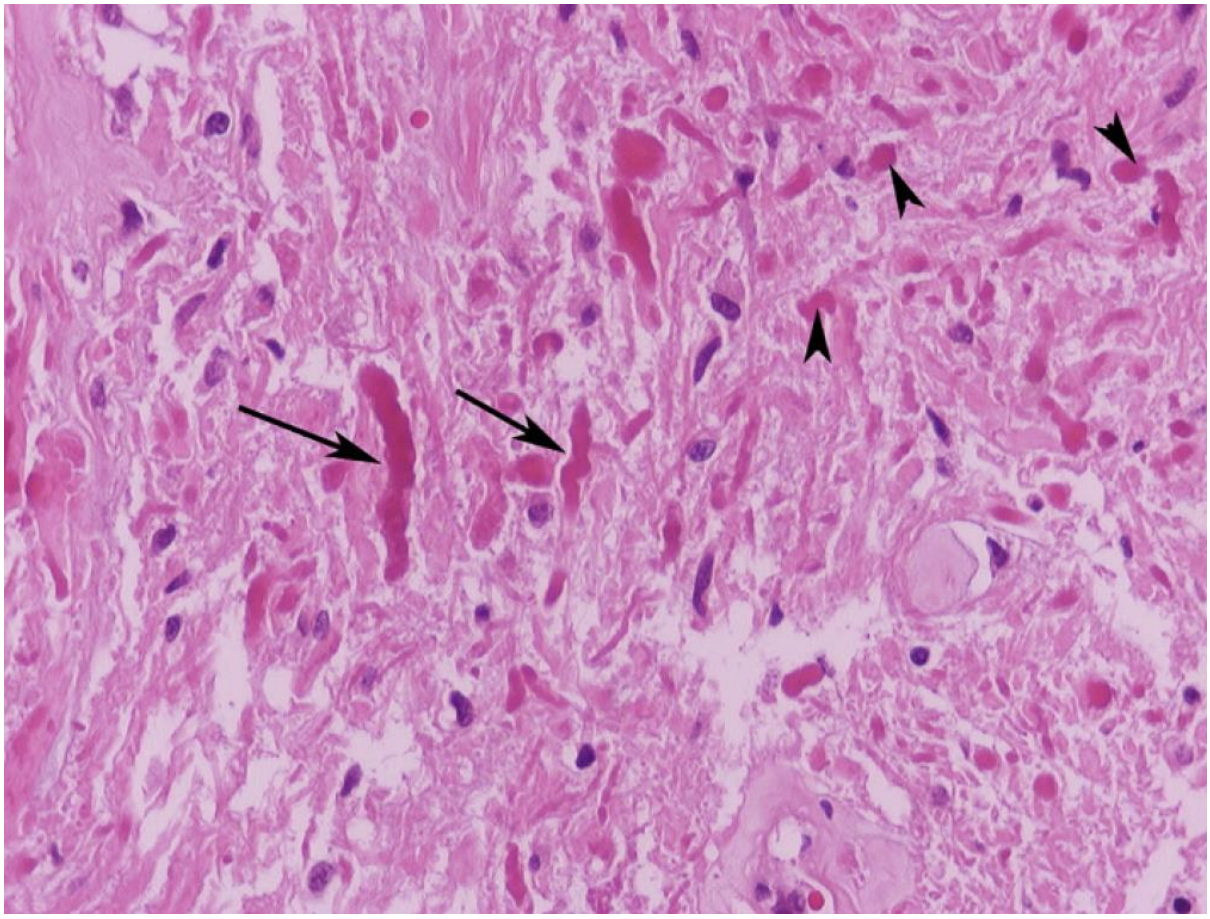

Figure 1.3: Commonly seen in PAs are Rosenthal fibres (arrows) and eosinophilic granular bodies (arrowheads) (H&E, 400x). [33]

The second component of PAs (Figure 1.4) is frequently hypocellular, susceptible to microcystic degeneration, exhibits multipolar tumour cells, and is accompanied by eosinophilic granular bodies. The microcystic areas can coalesce to form larger macrocysts. Eosinophilic granular bodies (Figure 3) are brightly eosinophilic intracytoplasmic inclusions comprising clusters of variable-sized granules displaying membrane-bound electron-dense structures. These bodies are not only present in PAs; they can also be seen in herring bodies, which are a common component of the posterior pituitary gland, as a result of vascular malformations and other neoplastic tumours, such as ganglioglioma, pleomorphic xanthoastrocytoma, and subependymal giant cell astrocytoma. [34]

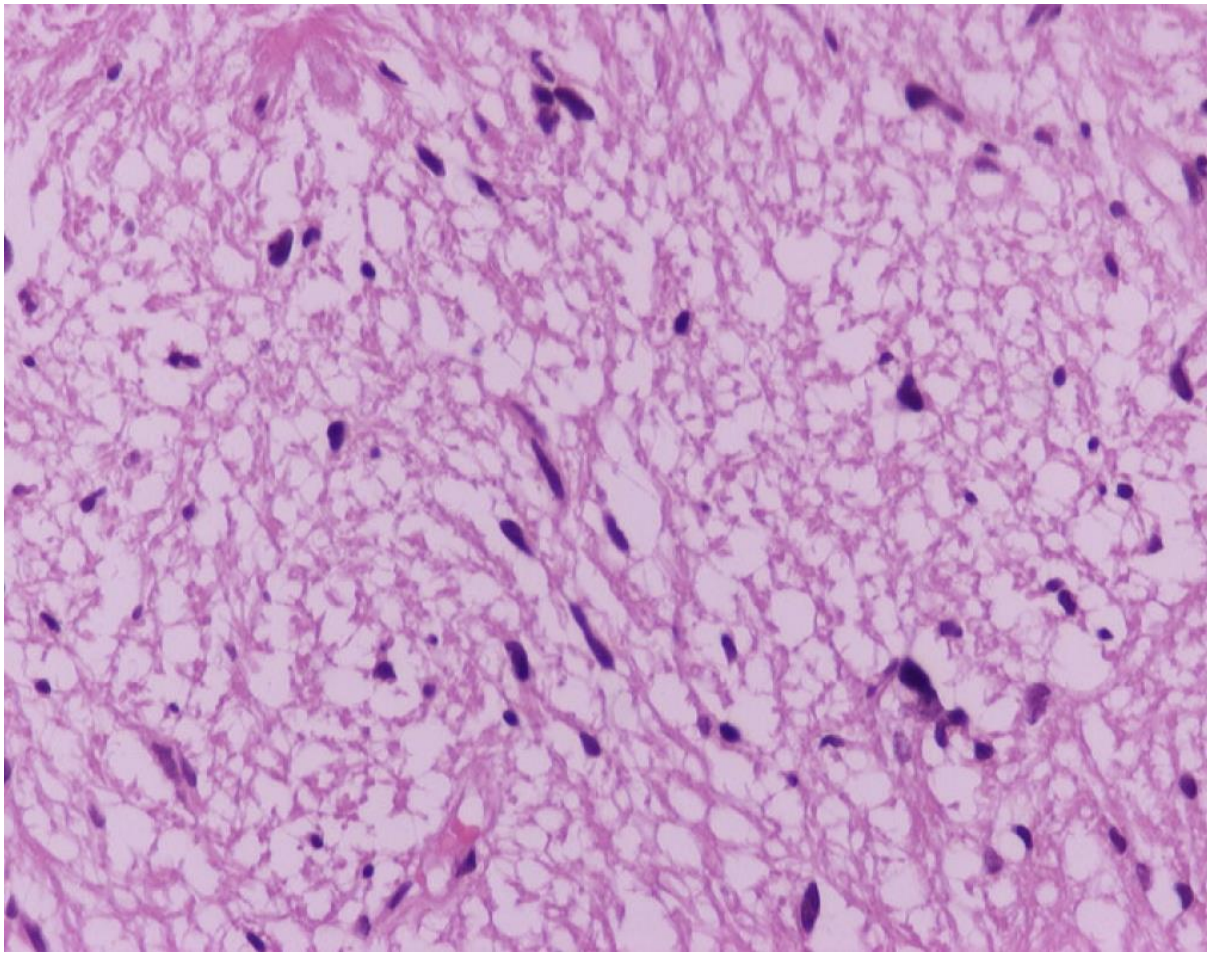

Figure 1.4: High magnification of the hypocellular, microcystic component (H&E, 100x). [33]

It is possible to notice worrying traits, which the WHO defines as PA with histological features of anaplasia. [17] However, this does not impact how the WHO classifies these tumours. These features include nuclear pleomorphism and hyperchromasia, brisk mitotic figures, infarct-type necrosis and glomeruloid vascular proliferation. [35,36] Rodriguez et al. [36] investigated 36 cases of PAs with anaplasia and concluded that these features mainly occur in the posterior fossa in adults.

These neoplasms are prone to degenerative changes, which include thick-walled hyalinised blood vessels, haemorrhage, myxoid change and calcification. [37] Some tumours may exhibit characteristics of pilomyxoid astrocytomas (PMAs, Figure 1.5A), which the WHO classifies as intermediate tumours due to their higher risk of recurrence and dissemination. [17] More myxoid matrix, the absence of biphasic zones with more monomorphous tumour cells, and an angiocentric (Figure 1.5B) distribution distinguish PMAs from PAs. [38]

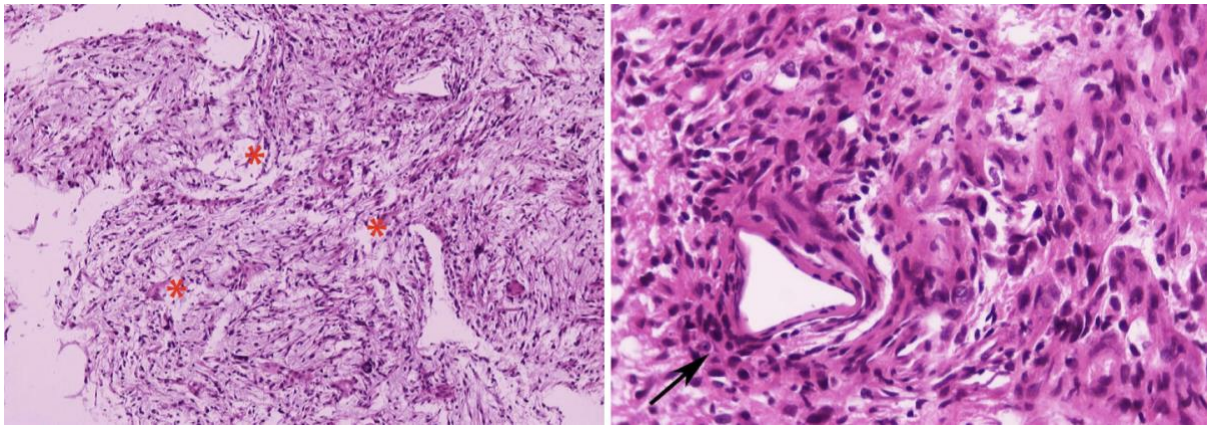

Figure 1.5: Pilomyxoid astrocytoma. A: Monomorphous tumour cells in a myxoid background (asterisks, H&E, 100x). B: Angiocentric arrangement of tumour cells (arrow, H&E,400x). [33]

1.2.3. Immunophenotype:

As expected, PAs arise from glial cells and are diffusely positive with the following immunohistochemical markers: glial fibrillary acidic protein (GFAP), S100 and SOX10. Neuronal markers are often negative, but the neuronal marker synaptophysin can be positive. CD34 is helpful since it usually shows no staining in PA and positive staining in tumours considered in the neuroradiological differential diagnosis, such as ganglioglioma.

PAs are not associated with isocitrate dehydrogenase 1 (*IDH1)* mutations; thus, IDH1 p.R132H expression is absent. Most tumours exhibit diffuse SOX10 and p16 positive staining, with PA and ependymoma being distinguished from one another by the presence of SOX10 and OLIG2 positive staining in PAs. [17] The proliferation index (Ki67) is usually less than 5%.

Monoclonal anti-BRAF V600E immunohistochemical stain is a surrogate marker for *BRAF* V600E mutation. This immunohistochemical marker is more often positive in craniopharyngiomas, gangliogliomas and pleomorphic xanthoastrocytoma.

The accuracy of tumour diagnosis has improved as a result of developments in molecular pathology techniques. One of these techniques includes fluorescence in-situ hybridisation (FISH), which has proven useful for confirming PAs. Simple assays, for instance, polymerase chain reaction (PCR), is accurate if one suspects a specific genetic alteration. These techniques are becoming more popular to correctly diagnose PAs.

1.3. Aetiology and pathogenesis:

1.3.1. General overview:

Advances in molecular studies have furthered our understanding of specific signalling pathway disturbances involved in tumour pathogenesis. The underlying cause of PA development is any biological process that leads to the activation and malfunctioning of the mitogen-activated protein kinase (MAPK) pathway. [39,40] To date, 70 genes encoding more than 200 distinct components comprise the MAPK system. [41]

1.3.2. Mitogen-activated protein kinase (MAPK) pathway:

MAP kinase pathway participates in signal transduction by delivering impulses to the cell nucleus that promote cell growth and division. [42] Under normal circumstances, most of the brain expresses MAPK/ERK signalling components. [21] This signalling system has been linked to the midbrain and cerebellum's development, cortical neurogenesis activation, and other neurological functions, including memory consolidation and pain perception. [43,44]

As shown in Figure 1.6, the MAPK pathway transmits impulses from outside the cell to the central region using a variety of protein kinases. [45] Signalling starts by binding of a ligand, often a growth hormone, to receptor tyrosine kinase (RTK). This results in the dimerisation of the two subunits of RTK. Downstream events are initiated, resulting in binding to *Rat sarcoma virus* (*RAS*), a monomeric G-protein. When bound to the nucleotide guanosine diphosphate (GDP), RAS is inactive; it only becomes active when GDP is replaced for guanosine triphosphate (GTP). [41]

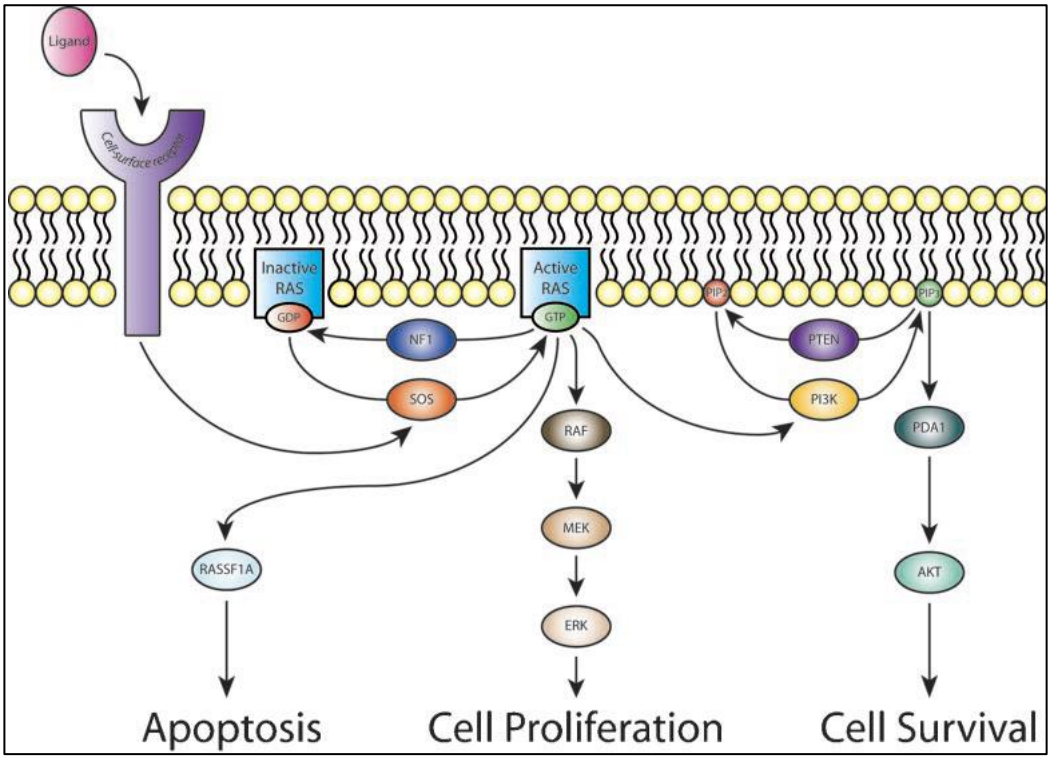

Figure 1.6: The major components of MAP kinase signal transduction pathway. [45]

In its active state, RAS can bind to several intracytoplasmic effector proteins, including *Rapidly accelerated fibrosarcoma (Raf);* another name is MAP kinase kinase. RAF kinases is a serine/threonine-specific protein kinases with three isoforms. These isoforms include Raf-1/c-Raf, B-Raf and A-Raf. [46] B-Raf has been described in the pathogenesis of numerous tumours, making this the most studied isoform. Activated B-Raf phosphorylates and activates the kinases MEK1/2 (also known as MAP kinase kinase), activating and phosphorylating ERK1/2 (another name is MAP kinase). Activated ERK can enter the cell nucleus and activate JUN and FOS, which are transcriptional factors. [42] Cell proliferation is triggered following the transcription of these target genes.

RAS is briefly activated by incoming signals, however, this is short-lived under normal circumstances. RAS activity is switched off when a conformational change occurs in guanosine phosphate. The MAP kinase signalling pathway is then turned off, resulting in the arrest of cell growth and differentiation.

Briefly, the MAPK cascade can be initiated by receptors other than RTK, for example, G-protein coupled receptors (GPCRs), through the process of cross-talk between signalling pathways. B-Arrestin modulates the GPCR pathway by recruiting various kinases, which in turn phosphorylates ERK. Once phosphorylated, ERK becomes activated, resulting in the

same downstream effects seen after its activation in the MAPK/RAS signalling pathway. [47]

In summary, regardless of the nature of the cellular stimulus, signal transmission is usually initiated by activating small G proteins or the interaction of upstream components of the cascade with adaptor proteins. Then, cytosolic protein kinases arranged in three to five levels continue to relay downstream cascade signals. [41] The kinases in each tier phosphorylate and activate the kinases located in their downstream tier to allow rapid and regulated transmission of signals to various cascade targets. [41]

1.3.3. Molecular biology of Pilocytic astrocytomas

Understanding the crucial signalling events underlying the development of PAs has improved significantly as a result of research efforts. The World Health Organisation (WHO) reports that all genomically studied PAs have shown genetic aberrations involving the MAP kinase signal transduction pathway. [23,39,40,48] Numerous reports found a correlation between clinicopathological features and genetic aberrations. [21] Compared to supratentorial tumours with a higher incidence of *BRAF V600E* mutations, infratentorial tumours frequently exhibit a high rate of *KIAA1549:BRAF* fusions. Worldwide interest has been in detecting PA-specific biological markers that might help predict the course of the disease.

Genetic alterations more specific to PAs include certain fusions and point mutations involving the following genes: *v-RAF murine sarcoma viral oncogene homolog B1 (BRAF), NF1, Ki-ras2 Kirsten rat sarcoma viral oncogene homolog (KRAS), Fibroblast growth factor receptor 1 (FGFR1)* and *Neurotrophic tropomyosin receptor kinase (NTRK).* [49–51]

A comparative analysis of PAs by Brokinkel et al. shows the relative distribution of genetic abnormalities compared to the anatomic site (Figure 1.7). [52] As indicated, the *BRAF-KIAA1549* gene fusion is the most frequent.

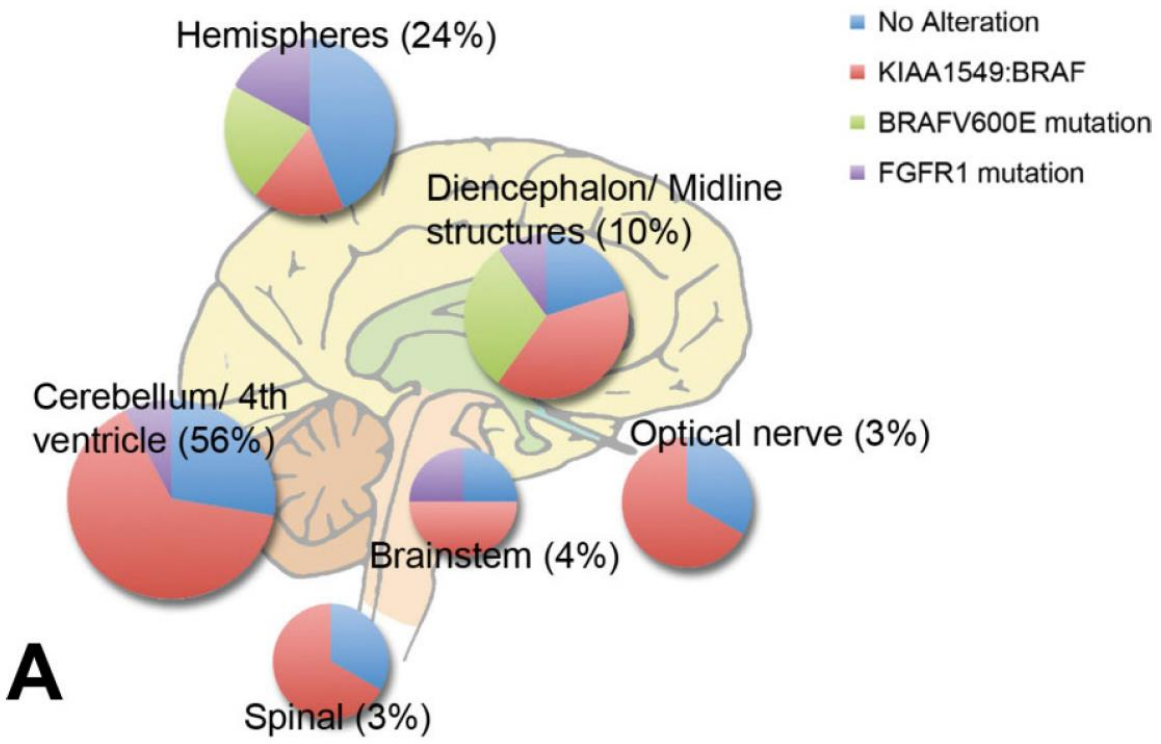

Figure 1.7: Diagrammatic demonstration of tumour location and its association with genetic alterations. [53]

BRAF mutations:

Cellular proliferation is one of the downstream effects that *BRAF* plays in the MAPK signalling pathway. *BRAF* genetic alterations have been divided into classes I, II and III based on these mutations' biochemical and signalling properties. [54,55] Classification of these mutations are essential to inform personalised anti-cancer treatment and predict response to MAPK-targeted therapies.

Smiech et al. [56] highlights the main characteristics of each mutational class in a simplified diagram (Figure 1.8). Class I comprise *BRAF V600E* mutations resulting in constitutively active monomers that signal independently from RAS. BRAF dimers with intense kinase activity form part of Class II *BRAF* mutations. Class III does not have kinase activity and is RAS-dependant.

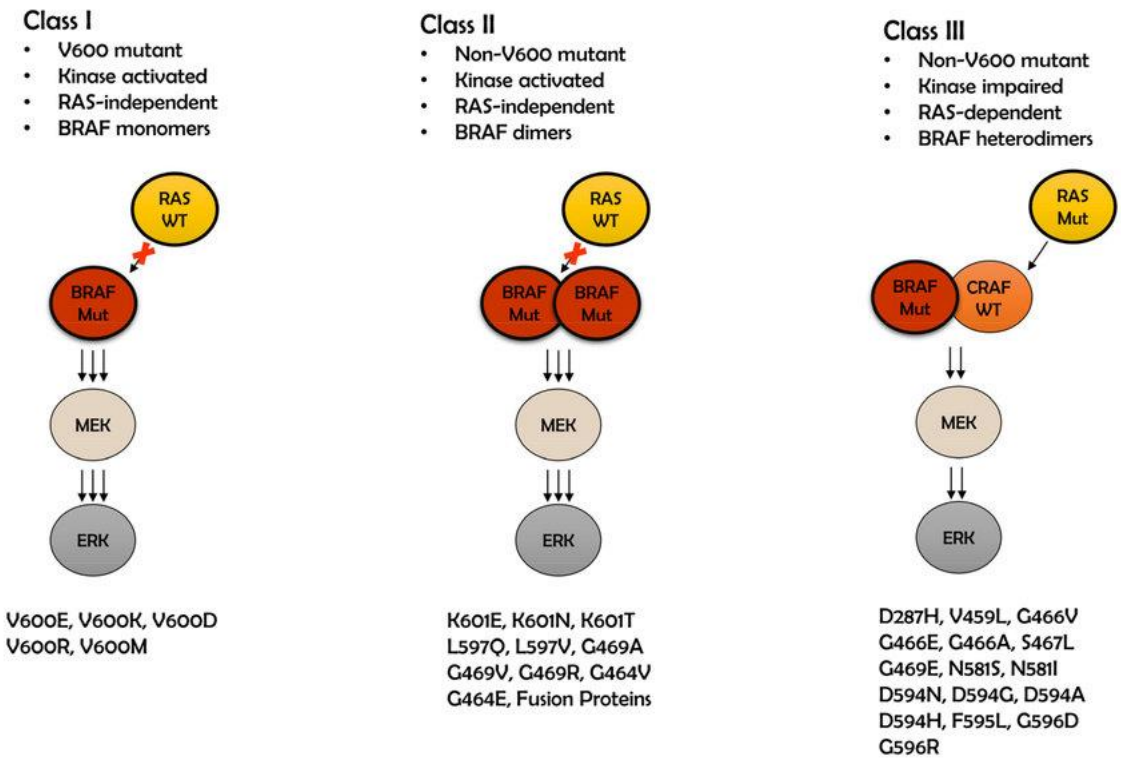

Figure 1.8: Class I, II and III *BRAF* mutational classification.[56]
Abbreviations: WT: wild type; Mut: mutation

Tandem duplication at chromosome 7q34, resulting in uncontrolled signal activation, which is categorised as a class II BRAF mutation, is the most frequent genetic anomaly reported in up to 60% of PAs. [1,57,58] A total of 5 different fusion combinations of the two genes have been described, i.e. *BRAF* exon 9 with *KIAA1549* exon 16 (comprising 60% of fusion events), *BRAF* exon 11 with *KIAA1549* exon 16, *BRAF* exon 9 with *KIAA1549* exon 15, *BRAF* exon 10 with *KIAA1549* exon 18 and *BRAF* exon 9 with *KIAA1549* exon 19.[59] More than one of these fusions, have been reported in some studies. [59,60] The *BRAF-KIAA1549* fusion is relatively specific to PAs and has not been reported in other entities. [21] This gene rearrangement can be a target for future treatment.

The second most common genetic change in PAs is *BRAF V600E* mutations where one amino acid, valine, is exchanged for another, glutamic acid, resulting in constitutive activation of the *BRAF* gene. This forms part of the class I *BRAF* mutations. [52,61] These genetic abberations are found in various other tumours, including craniopharyngiomas, pleomorphic xanthoastrocytomas, gangliogliomas, malignant melanoma, papillary thyroid carcinoma, colon carcinoma, cholangiocarcinoma, hairy cell leukaemia and multiple myeloma. [5,61]

KRAS mutations:

KRAS is a proto-oncogene that is vital in the MAP kinase signalling pathway. These mutations rarely occur in PAs.

1.4. Treatment

Treatment options are becoming more readily available and advanced as more research is done. The treatment of pilocytic astrocytomas and paediatric brain tumours, in general, requires a multidisciplinary team approach. Individualised therapy is advised and can range from surgery and radiotherapy to molecular-targeted interventions.

1.4.1. Surgery:

Complete surgical resection (CSR) is the cornerstone of PA treatment. The prognosis is good after the complete removal of these tumours; more than 90% of patients recover without further treatment, and the risk of recurrence decreases substantially in these patients. [62,63] Deeply situated, especially in the hypothalamus, large or infiltrative tumours are at risk for subtotal surgical removal. [64]

Many retrospective investigations assessed the likelihood of tumour recurrence, the need for adjuvant therapy, and prognosis after CSR. According to Sutton et al. [65], patients who received CSR had a recurrence probability of 1% as opposed to 79% for individuals who underwent subtotal tumour excision. Vassilyadi et al. [66] supported these findings, which reported no tumour recurrence in wholly resected tumours.

In conclusion, complete surgical removal of PAs significantly reduces tumour recurrence risk and contributes to excellent long-term survival rates. The need for additional treatment modalities in incompletely resected tumours has been controversial, with many conflicting reports.

1.4.2. Radiation:

As previously discussed, achieving complete surgical resection is curative; therefore, research studies have advised against radiation in these tumours. [67] In 1996, an article published by Campbell et al. [68] recommended deferring radiotherapy until proven that the tumour was progressive and surgically unresectable. However, the side effects caused by this treatment modality can harm the developing brain, causing functional and morphological alterations that eventually lead to cognitive deterioration. [69] Reports of other side effects include vascular events and secondary malignancies. [70,71]

According to Krishnatry et al. [67], patients who received upfront radiation experienced three- and four-fold increases in overall late mortality and tumour-related fatalities. Because of this, the WHO recommends radiation-sparing treatment to patients diagnosed with PAs. [23]

1.4.3. Molecular targeted therapy:

Genetic characterisation, known as molecular pathology, has become integral to routine health care in various neoplasms. This characterisation has enhanced diagnostic accuracy, more effective treatment stratification, and therapeutic efficacy monitoring. As mentioned, since most PAs have genetic abnormalities affecting the MAPK pathway, MEK inhibition is gaining popularity as a treatment modality. [23]

Figure 1.9, published by Dankner et al. [72] demonstrates the different classes of *BRAF* mutations and their proposed treatment. Wild-type *BRAF* gene is not mutated and forms part of the usual, non-cancerous MAPK signalling cascade. Class I, *BRAF V600E* mutations, forms BRAF monomers, resulting in RAS- independent unopposed downstream signalling. [72] As indicated, BRAF inhibitors (vemurafenib and dabrafenib) and MEK inhibitors (cobimetinib and dabrafenib) are two medications that can be used to target this pathway pharmacologically. [72]

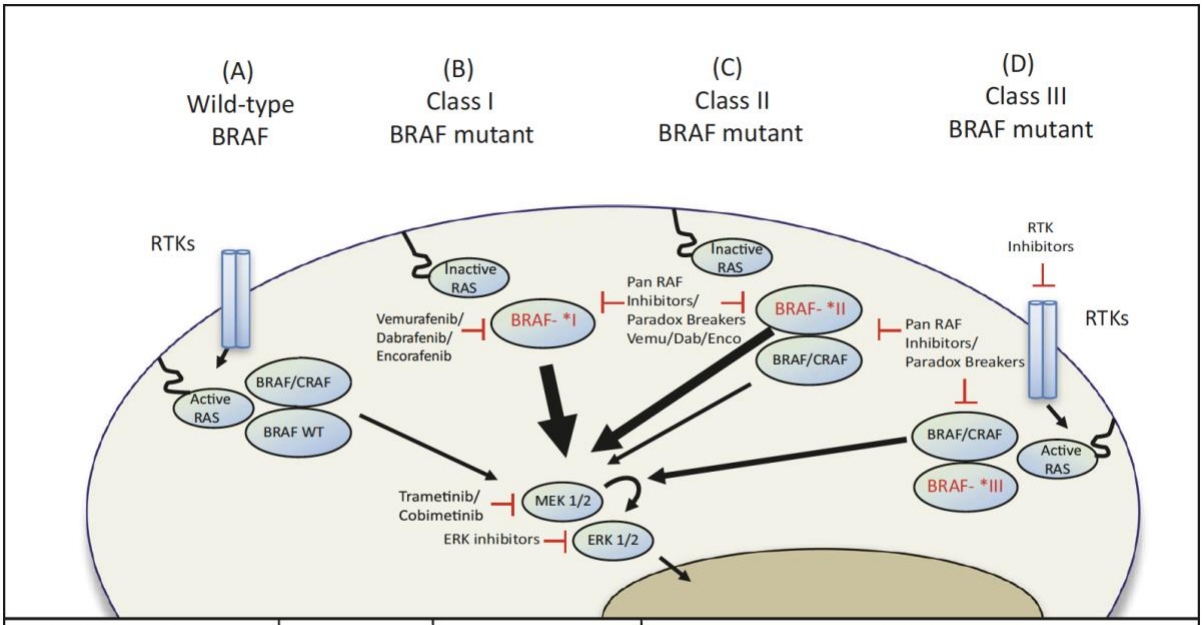

BRAF Mutant Class	Dimerization	RAS-Dependency	MAPK Targeted Agents Proposed
(A) Wild-Type BRAF	+	+	None
(B) Class I BRAF mutant	-	-	BRAF and MEK inhibitors*
(C) Class II BRAF mutant	+	-	MEK inhibitors (possibly with BRAF inhibitors)
(D) Class III BRAF mutant	+	+	MEK inhibitors + RTK inhibitors if no activated RAS

Figure 1.9: The proposed MAPK targeted treatment for each class of *BRAF* mutations. [72]

A retrospective study by Hawkins et al. [6] reported a link between *BRAF-KIAA1549* gene fusions and a good prognosis. PAs with *BRAF* gene missense mutations have shown reduced progression-free survival. [73] Other studies, however, found that the prognosis of PAs with *BRAF* rearrangements was not substantially distinct. [8,74]

In conclusion, few studies describe the long-term prognosis, and there are no accurate morphologic or molecular indicators of tumour behaviour or prognosis. However, larger cohorts are needed to provide a better understanding of PAs.

1.5. Future directives:

A minority of tumours are said to have a worse prognosis, despite the fact that total surgical resection can cure the majority of PAs. Certain clinical, radiological and molecular factors are culprits reported to result in an unfavourable outcome. Advances in molecular medicine made therapeutic options available to molecularly target tumours that demonstrate unfavourable prognostic factors. Given the higher morbidity associated with surgery and traditional chemo-radiation treatments, pharmaceutical blocking is a promising approach.

1.6. Rational for this study:

To date, no consistent markers are known to identify tumours that pursue an aggressive clinical course. This retrospective cohort study aims to look at the effect of specific *BRAF* genetic alterations on clinical behaviour and prognosis. If our alternative hypothesis proves true, this could open the door for early detection of tumours with a high recurrence risk and result in development of molecular directed therapy.

1.7. Aims and objectives:

- To evaluate the expression of BRAF using fluorescence in-situ hybridisation (FISH).
- To evaluate the immunohistochemical expression of BRAF.
- To evaluate BRAF-KIAA1549 fusion by using PCR.
- To compare the results with patient demographics and clinical outcomes.

Chapter 2

Materials and methods

2.1. Ethics approval:

The University of Cape Town Faculty of Health Sciences Human Research Ethics Committee gave their clearance for the conduct of this study (HREC: 440/2021) (Appendix 1).

2.2. Study design and cohort selection:

This was a retrospective cohort laboratory-based study. Convenient sampling was done at Red Cross Children's Hospital in Cape Town by searching the Division of Anatomical Pathology's electronic laboratory information database (Disa). The search included 69 cases of juvenile pilocytic astrocytomas diagnosed between January 1984 and December 2016. Both formalin-fixed paraffin wax-embedded (FFPE) tissue blocks and adequate clinical follow-up were available. All relevant information, including age (ranging from birth to 13 years of age), tumour site and treatment received, and tumour recurrence, was captured in a database. Each case was assigned an arbitrary case number to anonymise the data and protect patient confidentiality. After that, the tissue blocks were retrieved from archives of the Division of Anatomical Pathology at Red Cross War Memorial Children's Hospital. Archived stained slides of all the cases were reviewed for adequacy, and two investigators confirmed the diagnosis. Cases with minimal tumour tissue that were likely to cut away on deeper sections and/or necrosis were excluded.

2.3. Immunohistochemistry:

Sections of the FFPE tissue blocks were cut at 4 microns with a manual rotatory microtome, mounted on adhesive glass slides and allowed to dry at 60°C for one hour. The EZ Prep solution (Ventana Medical Systems, Tuscon, AZ, USA) was used to visualise and rehydrate the FFPE slides. The next step included 64 minutes of heat pretreatment for antigen retrieval using cell conditioning solution. As per the manufacturer, immunohistochemical staining was performed using the Ventana BenchMark XT immunostainer (Ventana Medical Systems, Tuscon, AZ, USA) and visualised using the OptiView DAB IHC Detection Kit (Ventana Medical Systems, Tuscon, AZ, USA). The slides were incubated at 36°C for 40 minutes with primary BRAF V600E (VE1) specific monoclonal antibody (Ventana Medical Systems, Tuscon, AZ, USA). This step was followed with another round of incubation after adding OptiView HQ Universal Linker and OptiView HRP Multimer. Counterstaining was performed with one drop

of haematoxylin and one drop of blueing reagent. Lastly, the slides were dehydrated using increasing concentrations of ethanol, cleared in xylene and sealed using a Dako mounting medium (Perlan, Inc., Santa Clara, CA, USA).

Light microscopic examination followed by using positive and negative controls as a reference guide. Cases were positive when unequivocal cytoplasmic staining of uniform intensity was seen while using a case of papillary thyroid carcinoma with a *BRAF V600E* mutation. Cases were regarded as negative when there was an absence of staining, nuclear positive staining or staining in the non-tumour cells. The immunoreactive positive cases were scored as weak (1+), moderate (2+), or strong (3+) based on the intensity of staining in tumour cells (Table 2.1).

Table 2.1: Scoring guide for the BRAF V600E immunohistochemistry

	Proportion Score	Stained cell per area
Negative	0	No cytoplasmic staining
Weak	1+	1-25%
Moderate	2+	26-50%
Strong	3+	51-100%

2.4. Fluorescence in situ hybridisation:

FFPE tissue sections of 4um were cut and mounted on adhesive glass slides. The slides were left to bake in a dry incubator overnight. The following day, the slides were dewaxed, rehydrated and air-dried following pretreatment in HCl at 37° for 20 minutes (Appendix 2). After that, antigen retrieval was achieved using sodium thiocyanate at 80°C for 30 minutes. The tissue was then digested using HCl-pepsin at 37°C for 10 minutes. The ZytoLight SPEC BRAF Dual Colour Break Apart Probe (ZytoVision, Bremerhaven, Germany) (Figure 2.1) was applied (5ul) to each section. The section was coverslipped and sealed with rubber cement. The slides were placed in a hybridisation oven for denaturation at 75°C for 5 minutes, followed by hybridisation at 37°C for 18-24 hours. After hybridisation, the slides were washed in post-hybridisation buffer (2x SCC/0.3%IGEPAL CA-630) for 2 minutes and 10 seconds at 72°C. DAPI (4',6-diamidino-2-phenylinodole) was applied, the slides were coverslipped and sealed with clear nail varnish. The slides were viewed using a fluorescence microscope with the appropriate excitation and emission filters. For each case, at least 100 non-overlapping cells were counted. The cases that did not have a BRAF rearrangement showed two separate green and orange signals. In cells with chromosomal aberrations, a different signal pattern comprised an independent green and orange single and a paired green/ orange (yellow) signal

indicative of gene fusion was observed.

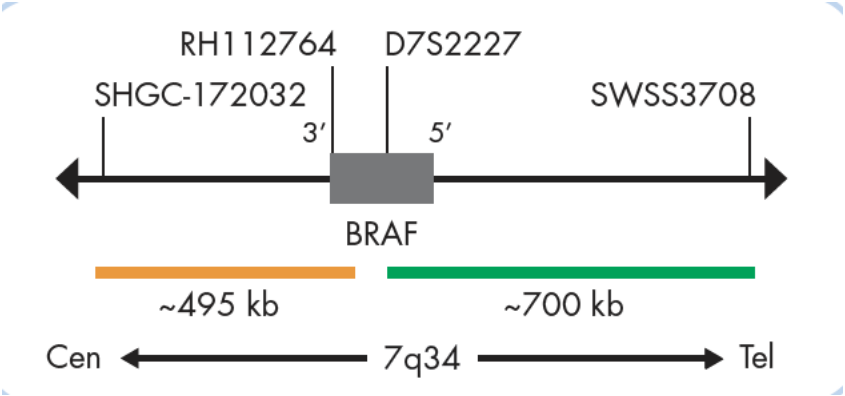

Figure 2.1: SPEC BRAF probe map.

2.5. RNA extraction:

At least 3 FFPE tissue sections, cut at 5µm, were used for the RNA extraction. The High Pure RNA Paraffin Kit (Roche Diagnostics GmbH, Mannheim, Germany) was used according to the manufacturer's instructions. Briefly, the process was as follows: the first day comprised tissue dewaxing and digestion; this was started by decontaminating the working environment and equipment. A labelled 1.5ml microcentrifuge tube was allocated to each sample and extraction control. 600µl of xylene was added to each tube, and after that, the tissue was scraped off the slide with a scalpel blade and added to the tube. This was mixed using a vortex, after which the samples were incubated at room temperature for 5 minutes. 300µl of ethanol (96-100%) was added to each tube and mixed again. The samples were centrifuged at 13000 revolutions per minute (rpm) for 2 minutes to pellet the tissue and remove the supernatant. After that, 900µl ethanol was added to the pellet, vortexed and centrifuged again at the same speed. The next step was to ensure evaporation of the alcohol by incubating the open microcentrifuge tube at 55°C for 10 to 15 minutes. The tubes were covered with a clean paper towel and allowed to dry. Tissue digestion followed by adding 100µl of tissue lysis buffer, 16µl of 10% SDS, and 40µl of proteinase K working solution to each tube. The tubes were incubated overnight at 55°C on a heating block.

The second day started with the decontamination of the work area and equipment. Initially, 325µl of binding buffer and an equal volume of absolute ethanol were added to each lysate. The contents were mixed and then transferred to a filter or collection tube and allowed to centrifuge for 30 seconds at 8000g. The flow-through was discarded, and the filter was transferred to a clean collection tube. It was centrifuged at 13000rpm for 2 minutes to allow the drying of the filter. After that, 500µl of wash buffer 1 was added. This was followed by centrifugation, and the process was repeated by adding 500µl followed by 300µl of wash buffer

2. During each step, the flow-through was discarded. The filter was then placed in a new 1.5ml microtube, and a 90µl elution buffer was added. It was centrifuged at 8000g for 1 minute. The filter was discarded, and the eluate was mixed with 10µl DNase incubation buffer and 2µl of DNase I working solution. The sample was incubated for 60 minutes at 37°C. After that, 20µl of tissue lysis buffer, 18µl of 10% SDS and 40µl proteinase K working solution were added to each sample and gently mixed by vortexing. The samples were incubated for 1 hour at 55°C on the heating block. After that, 325µl of binding buffer and an equal volume of absolute ethanol were added to each lysate. The contents were mixed and then transferred to a filter or collection tube and allowed to centrifuge for 30 seconds at 8000g. The washing process was repeated. Finally, the RNA was eluted by adding 50µl of elution buffer. The RNA was kept on ice for the cDNA synthesis and stored at -20ºC.

2.6. Spectrophotometry:

A Nanodrop spectrophotometer (Thermo Fisher Scientific, USA) was used to determine the purity (measured as A260/ A280 ratio) and concentration (ng/µl) of RNA of each case by assessing the ultraviolet-visible spectrum absorbance. Nucleic acids have an absorption maximum of 260 nm and proteins of 280 nm. The process started by selecting the desired application (RNA) on the Nanodrop software and blanking the instrument with an elution buffer. Two microliters of each sample were measured. The RNA yield was calculated based on absorbance at a wavelength of 260 nm (A260nm unit of RNA equals 40µl/ ml H2O). The Nanodrop spectrophotometer provided an A260/A280 ratio that was used to assess the purity of the sample. A sample was regarded as pure when the ratio was 2.

2.7. cDNA synthesis:

The cDNA synthesis process was started by decontaminating the work area and equipment. The Quantitect Reverse Transcription kit (Qiagen; USA) was used per the manufacturer's protocol. For each sample, 12µl of RNA template was added to 2µl of genomic DNA (gDNA) wipeout buffer in a 0.2ml PCR tube. These samples were incubated at 42°C for 2 minutes. After that, 1µl of Quantiscript Reverse Transcriptase, 4µl of Quantiscript Reverse Transcriptase Buffer and 1µl of Reverse Transcriptase Primer Mix were added to each tube. The samples were then incubated at 42°C for 15 minutes. The samples were ready for polymerase chain reaction (PCR) after final incubation at 95°C for 3 minutes to ensure reverse transcriptase inactivation.

2.8. Polymerase chain reaction:

The PCR master mix was prepared using the Faststart DNA Taq Polymerase Kit (Roche Diagnostics; Mannheim, Germany) according to manufacturer instructions. The reagents were

thawed and briefly centrifuged before the reaction was set up. A master mix of the total number of reactions was made. The following reagents were added to a sterile labelled 1.5ml microcentrifuge tube: PCR-graded water, PCR Buffer, Magnesium chloride, dNTP (deoxynucleoside triphosphate including all four nucleotides), forward and reverse primers (Table 2.2), and Faststart Taq DNA Polymerase. This was mixed and dispensed (23µl each) in labelled 0.2ml PCR tubes. Two microliters of cDNA were added to each tube. Appropriate positive and non-template controls were included in each PCR assay. The tubes were placed in a thermal cycler, and PCR was performed (Table 2.2).

Table 2.2: Primer sequences and PCR conditions

Name	Primer	Sequence 5'–3'	PCR conditions	Positive control	Product (bp)
B-Actin	ACTB-F	AGCTGTCACATCCAGGGGTCCTCAC	*1x [95^{o}C 5 min] 45x [95^{o}C 30 sec; 60^{o}C 30 sec; 72^{0}C 30sec] 1x [72^{o}C 7min]*	Previously tested sample	206
	ACTB-R	CGGACTCGTCATACTCCTGCTTG			
KIAA1549-BRAF	KIAA1549 Exon 16 F	GCACGCCAGACCATGCACTC	*1x [95^{o}C 5 min] 40x [95^{o}C 30 sec; 57^{o}C 30 sec; 72^{0}C 30sec] 1x [72^{o}C 7min]*	gBlock control (Appendix 2)	228 or 402
	BRAF Exon 11 R	ACTCGAGTCCCGTCTACCAAG			

Abbreviations: bp, base pairs; min, minutes; sec, seconds

The positive control for the *KIAA1549-BRAF* PCR comprised a synthetic double-stranded DNA fragment (gBlock) manufactured by Integrated DNA Technology (Appendix 2). Only those cases that were positive for the reference gene, β-Actin, were subject to the *KIAA1549-BRAF* PCR. A fusion product of *KIAA1549* Exon 16F with *BRAF* Exon 11 R will give you a product with 402bp, whereas a fusion product of *KIAA1549* Exon 16F with *BRAF* Exon 9 R will give a product with 288bp.

2.9. Agarose gel electrophoresis:

Following PCR, the products were separated on a 1.5% agarose gel (Appendix 2). Briefly, the prepared gel was placed in the tank containing 1xSB buffer. The samples were prepared by mixing 12µl PCR product with 2µl loading dye. Each sample was loaded into a separate well of the gel. A ready-to-use molecular weight marker was added to the last well. The tank lid was placed carefully on the tank, and the gel was run at 180V for 40 minutes. After that, the power supply was disconnected; the gel was removed from the tank and placed on a gel documentation system UV transilluminator for analysis. The gel was photographed, and the printed image was annotated.

2.10. Statistical analysis:

STATA version 17.0 (Stata Corporation, College Station, Texas, USA) and R (version 4.2.1; R Core Team, Vienna, Austria) were used to conduct the statistical analyses. The proportions described in the study were reported as median percentages with interquartile ranges. Using Wilcoxon rank-sum tests and the Chi-squared/Fisher's exact test, the variations among the risk categories were compared. Associations between tumour recurrence and anatomical site were assessed using binomial regression. Results were presented as risk ratios with 95% confidence intervals (CIs). A p value <0.05 was considered statistically significant. Missing values were excluded from the analyses.

Chapter 3

Results

Appendix 3 shows a composite table of data captured and generated during this study.

3.1. Demographic Characteristics

The patients in this study were six years old on average (interquartile range, IQR: 3 - 9) (Table 3.1). There was one patient aged under 12 months; an equal proportion of patients in the 1 - 5-year age group, n=27 (39.1%) as well as the 6 - 10-year age group, and 11 (15.94%) patients aged 11 - 15 years old. Fifty-six (56) patients had data on gender available, and this included 21 (30.43%) male and 33 (47.83%) female. Clinical data on patient gender was absent in 15 cases.

Table 3.1: Study Population Characteristics

	Total (N=69)
Age (Years)	
<1	1 (1.45)
1-5	27 (39.13)
6-10	27 (39.13)
11-15	11 (15.94)
Missing	3 (4.35)
Median (IQR)	6 (3 - 9)
Gender	
Male	21 (30.43)
Female	33 (47.83)
Missing	*15 (21.74)*

3.2. Anatomical Distribution

Figure 3.1 depicts the major anatomical distributions of PA in this cohort. The neoplasm presented in the infratentorial compartment in 43 (62.32%) cases, with the majority occurring in the cerebellum. In contrast, 23 (33.34%) patients had supratentorial tumours, of which 13

(18.84%) presented in the cerebral hemisphere, 6 (8.7%) in the diencephalon and 4 (5.8%) in the optic chiasm/tract. Three cases had no anatomical site specified.

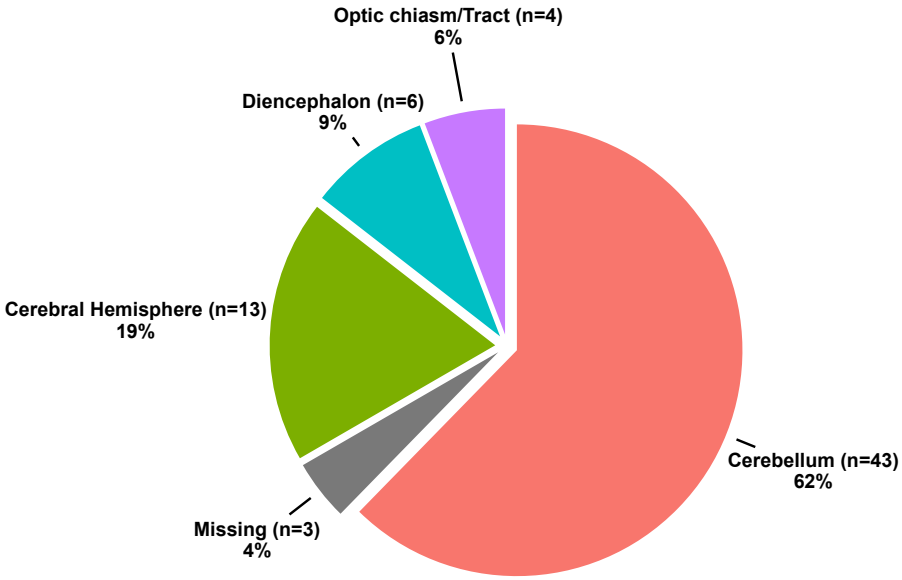

Figure 3.1: Tumor Distribution by Anatomic Location

Figure 3.2 demonstrates this study's major anatomical distributions stratified by age group. Essentially all children below the age of one year presented with tumours in the cerebellum. We report a relatively equal distribution of cerebellar and cerebral tumours in children between the ages of 11 and 15 years.

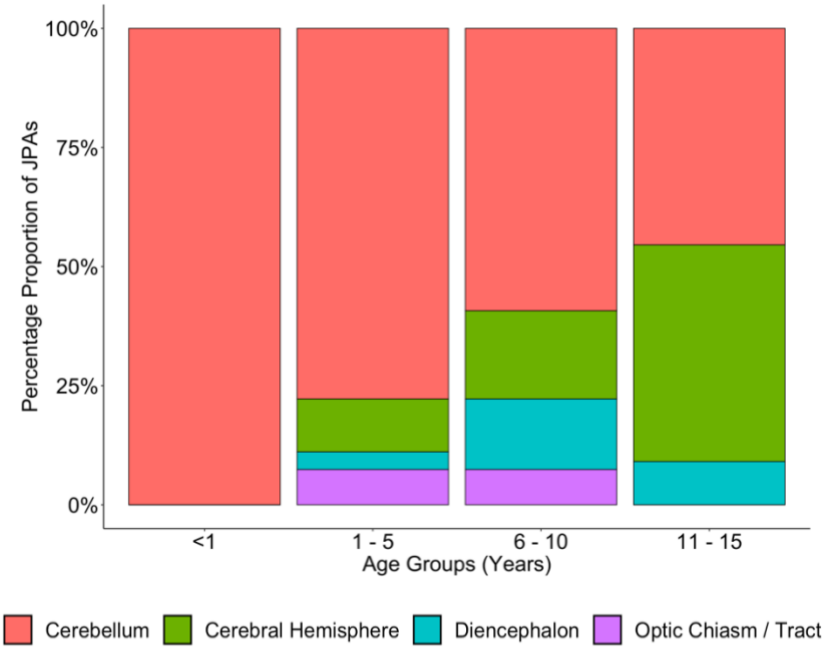

Figure 3.2: Anatomic Distribution of Tumor in Different Age Groups

Table 3.2 summarises the major anatomical distributions of PA tumours stratified by gender. There were no significant differences when comparing the anatomical site by gender.

Table 3.2: Anatomic Distribution of Tumor Stratified by Gender

	Male	Female	pValue
			0.48
Cerebellum	13 (61.90)	21 (67.74)	
Cerebral Hemisphere	4 (19.05)	6 (19.35)	
Diencephalon	3 (14.29)	1 (3.23)	
Optic chiasm/Tract	1 (4.76)	3 (9.68)	

3.3. Tumour Recurrence:

Evidence of tumour recurrence occurred in 20 (29%) patients. A comparison between the rates of recurrence in the infratentorial and supratentorial anatomical compartments showed higher rates of recurrence in the supratentorial compartment, which was statistically significant (p=0.005) (Table 3.3).

Table 3.3: Risk of tumour recurrence and distribution as per infratentorial and supratentorial compartment

		No recurrence	Recurrence	pValue
Site				0.005
	Infratentorial	35 (76.09)	8 (40.00)	
	Supratentorial	11 (23.91)	12 (60.00)	

A comparison of the relative risk of tumour recurrence by anatomical site based on an unadjusted model demonstrated that supratentorial tumours are more likely to recur when compared to tumours in infratentorial compartment RR 2.80 (95% CI: 1.34 - 5.86) and this was statistically significant (p=0.006) (Table 3.4).

Table 3.4: Risk ratio of tumour recurrence and distribution as per infratentorial and supratentorial compartment

	Risk Ratio (95% CI)	pValue
Site		
Ref: Infratentorial	1.0	-
Supratentorial	2.80 (1.34 - 5.86)	0.006

Figure 3.3 depicts the recurrence rates in each of the major anatomical distributions of PA.
Recurrence rates:

- Of the total 43 cases in the cerebellum, 8 (18,6%) were recurrent.
- Of the total 13 cases in the cerebral hemisphere, 8 (62%) were recurrent.
- Of the total 6 cases in the diencephalon, 3 (50%) were recurrent.
- Of the total 4 cases in the optic chiasm/tract, 1 (25%) was recurrent.

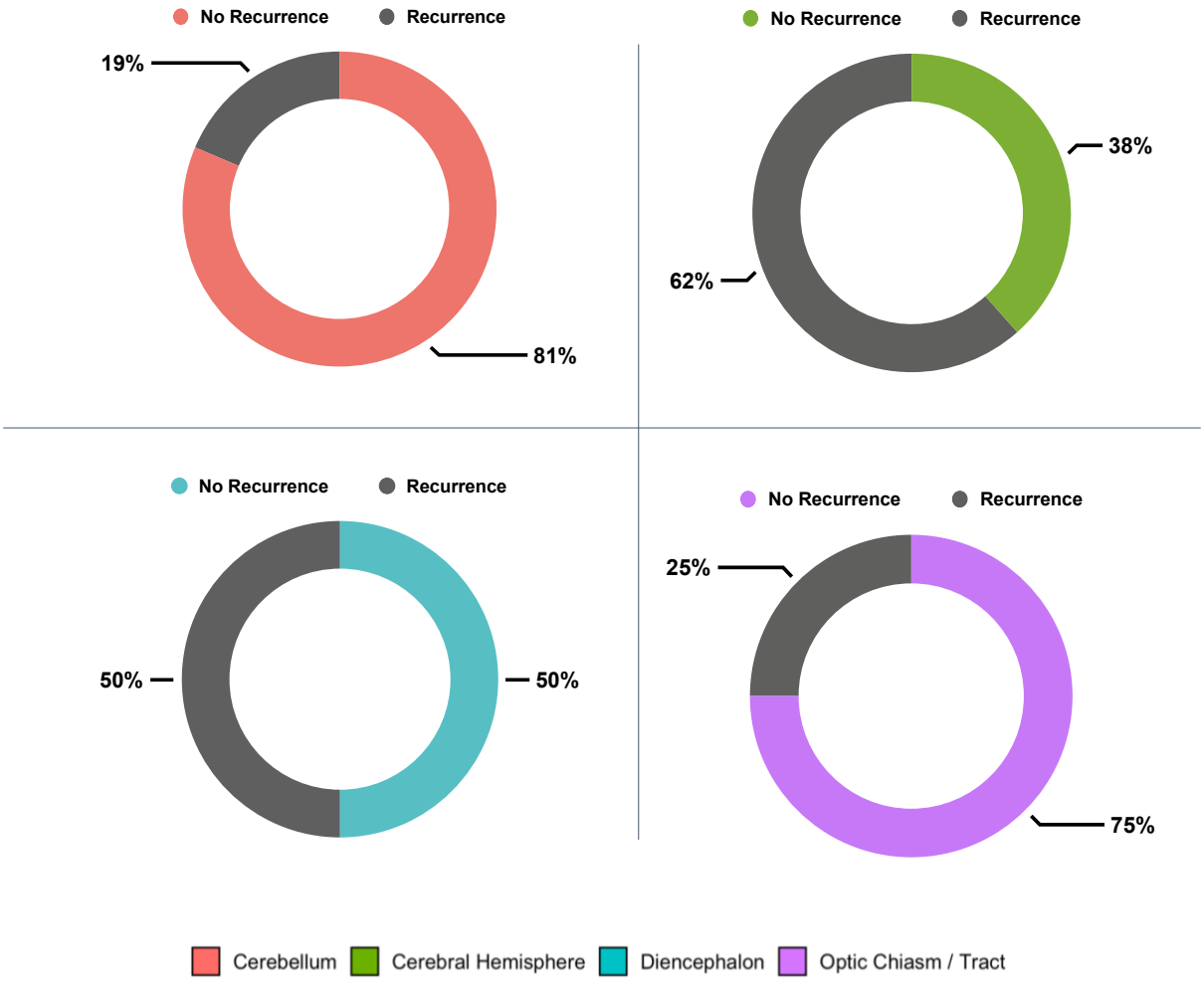

Figure 3.3: Rates of Recurrence in Tumour by Anatomic Location Groups

When further stratified by anatomical site within the compartments (Table 3.5), compared to the cerebellum, tumours in the cerebral hemisphere are 3.3 times more likely to recur (95% CI: 1.55 – 7.06; p=0.002). The risk was borderline significantly higher in the diencephalon (p=0.056).

Table 3.5: Risk of Tumour Recurrence by Anatomical Site

	Risk Ratio (95% CI)	pValue
Site		
Ref: Cerebellum	1.0	-
Cerebral Hemisphere	3.31 (1.55 - 7.06)	0.002
Diencephalon	2.69 (0.97 - 7.42)	0.056
Optic chiasm/Tract	1.34 (0.22 - 8.20)	0.749

There was no significant difference when comparing the tumour recurrence rate with tumour resection or debulking (Table 3.6). .

Table 3.6: Comparison of the risk of recurrence in tumours receiving complete vs incomplete surgical resection

	Incomplete surgical resection (N=9)	Complete surgical resection (N=46)	pValue
			0.58
No recurrence	5 (55.56)	30 (65.22)	
Recurrence	4 (44.44)	16 (34.78)	

Table 3.7 demonstrates the risk of tumour recurrence according to patient age (n=66). In this cohort, we report no significant difference in tumour relapses compared to patient age. There were 3 patients who had no data on clinical age, of which 2 presented with no tumour recurrence and 1 had recurrence.

Table 3.7: Tumour recurrence stratified according to age

	Age (Years)				
	<1	1-5	6-10	11-15	pValue
					0.7
No recurrence	1 (100)	17 (62.96)	20 (74.07)	8 (72.73)	
Recurrence	0 (0)	10 (37.04)	7 (25.93)	3 (27.27)	

3.4. BRAF Immunohistochemistry:

Of the 69 patient tumours, 46 showed absent cytoplasmic staining with the monoclonal anti-*BRAF V600E* immunohistochemical stain (Figure 3.4 B). At the same time, 23 samples had insufficient tumour content to perform analysis. We used papillary thyroid carcinoma as a positive control (Figure 3.4 A). Non-specific nuclear positive staining (Figure 3.4 C) and hemosiderin-laden macrophages (Figure 3.4 D) were regarded as false positive staining and disregarded.

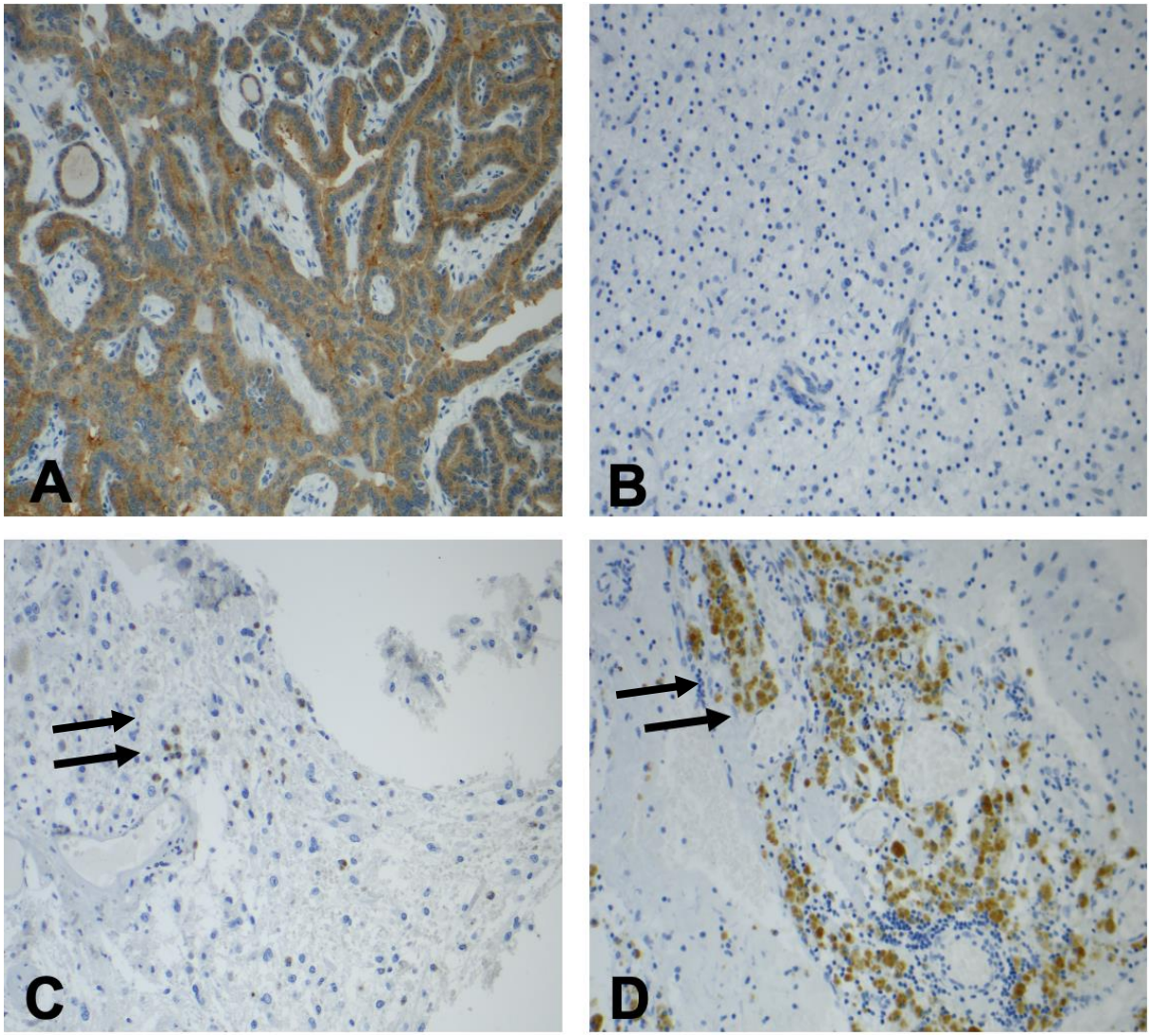

Figure 3.4: Immunohistochemical staining for *BRAF V600E* antibody. (A) Papillary thyroid carcinoma was used as a positive control (H&E, 200x). (B) Negative cytoplasmic staining in tumour cells (H&E, 200x). (C) Non-specific nuclear staining (arrow) and (C) hemosiderin-laden macrophages (arrow) were regarded as negative staining (H&E, 200x).

3.5. FISH for *BRAF-KIAA1549* fusion:

Among the 69 cases included in this series, 35 (50,7%) were submitted for fusion analysis, while 34 (49,3%) were excluded due to insufficient tissue or loss of tissue during processing. In a normal brain cell, without translocation, two green and two orange signals are identified (Figure 3.5). None of the 35 processed samples showed *BRAF-KIAA1549* gene rearrangement (Figure 3.6).

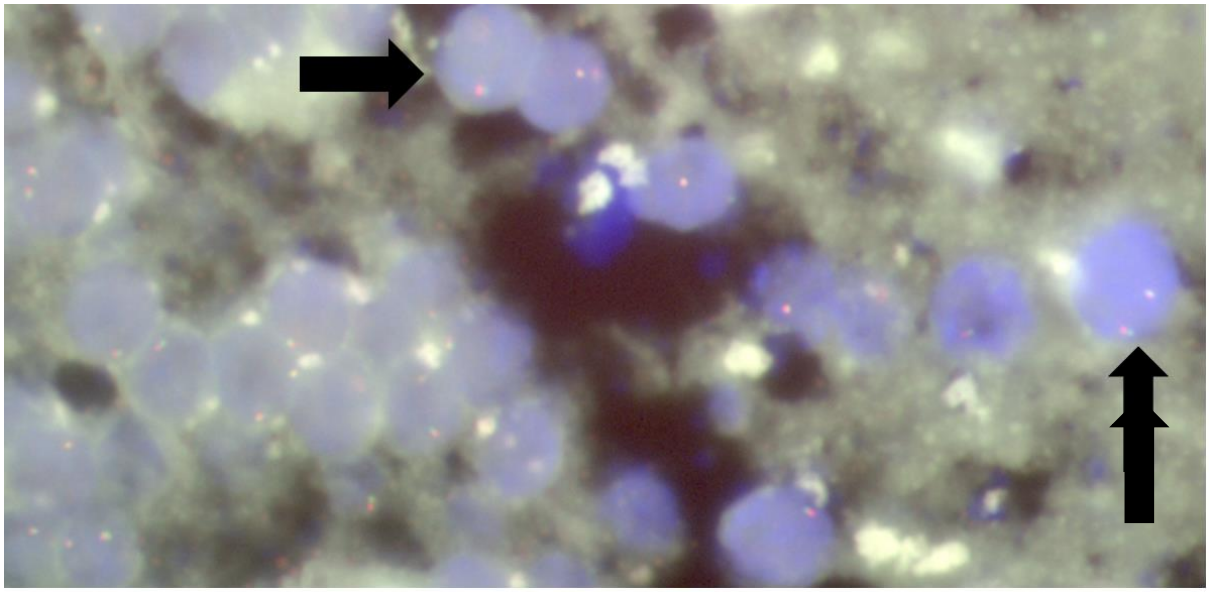

Figure 3.5: *BRAF-KIAA1549* FISH analysis in normal brain (without a translocation) illustrated by two green and two orange (arrows) signals in every cell.

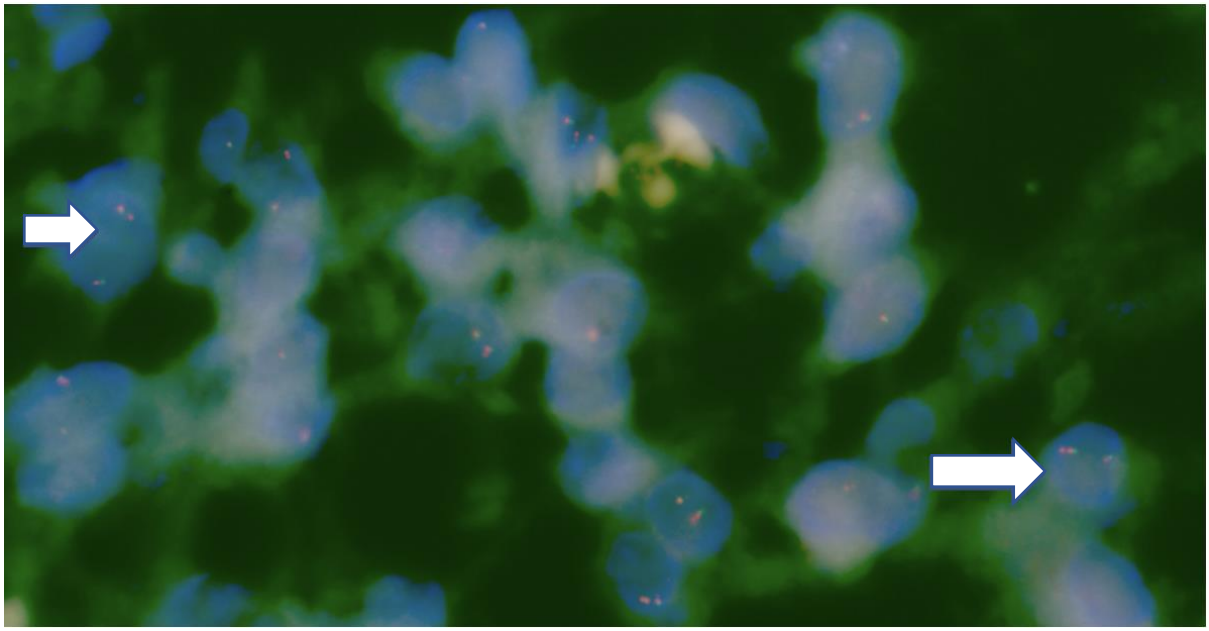

Figure 3.6: Representative image of a *BRAF-KIAA1549* fusion negative PA (two orange and two green signals, arrows) reported in this series.

3.6. RNA Extraction:

RNA was extracted from 32 cases (Appendix 4). The quantity and purity of each case is also demonstrated (Appendix 4). The spectrophotometer readings showed a yield of between 1.10-436.10ng/ul. The ratio of absorbance at 260nm (A260) and 280nm (A280) was used to assess

the purity of RNA. In our cohort, this ratio ranged from 1.20-2.04. Contamination by, for instance, organic compounds might explain the lower ratio reported in some samples. This did, however, not affect the subsequent step of cDNA synthesis.

3.7. Beta actin PCR for cDNA:

Figure 3.9 depicts ethidium bromide-stained gel showing the Beta actin PCR products. The size of the product is 206 base pairs. We report a good signal via Beta actin PCR in all the cases submitted for *BRAF-KIAA1549* fusion PCR.

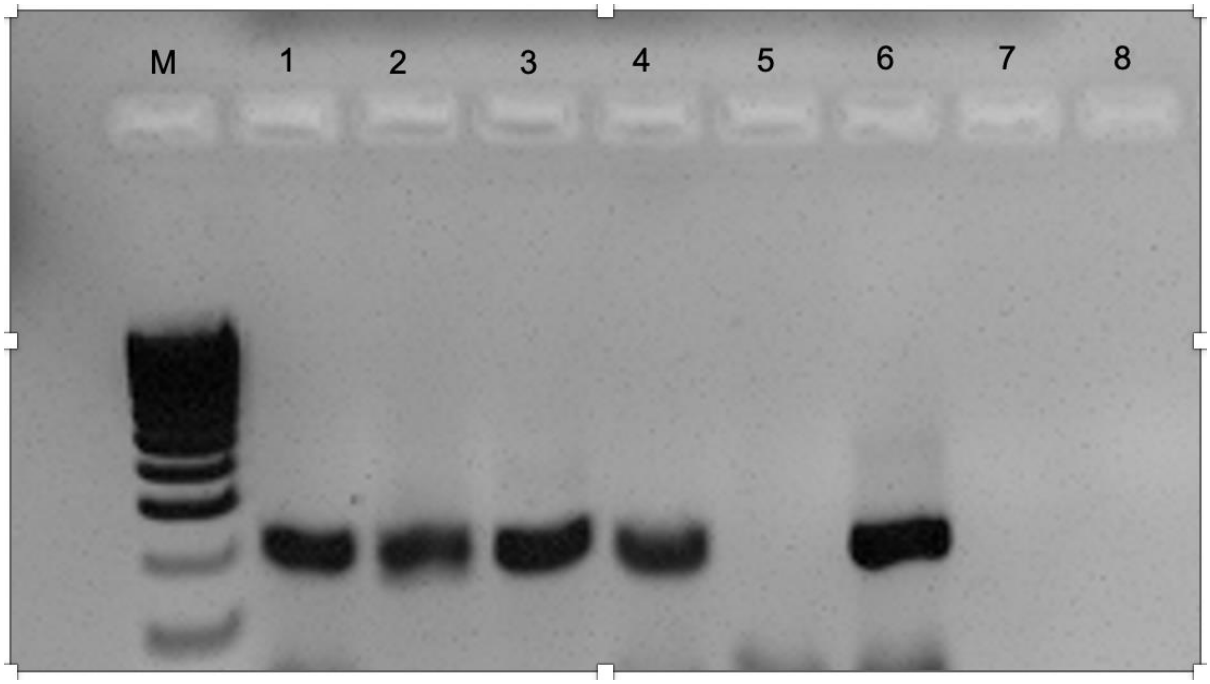

Figure 3.7: Ethidium bromide-stained gel showing the Beta actin PCR products. The size of the product is 206 base pairs. Lane M indicates the DNA ladder (by molecular weight). Lanes 1 to 4 represent positive cases. Lane 5 is the extraction control. Lane 6 the positive control. Lane 7, negative control.

3.8. PCR for BRAF-KIAA1549 fusion:

BRAF-KIAA1549 fusion PCR product is depicted in Figure 3.8, using an ethidium-bromide-stained gel. The product size is 228 or 402 base pairs depending on the fusion present. RT PCR from 32 RNA extracted FFPE samples followed by amplicon sequencing detected no fusion transcripts in any of the cases.

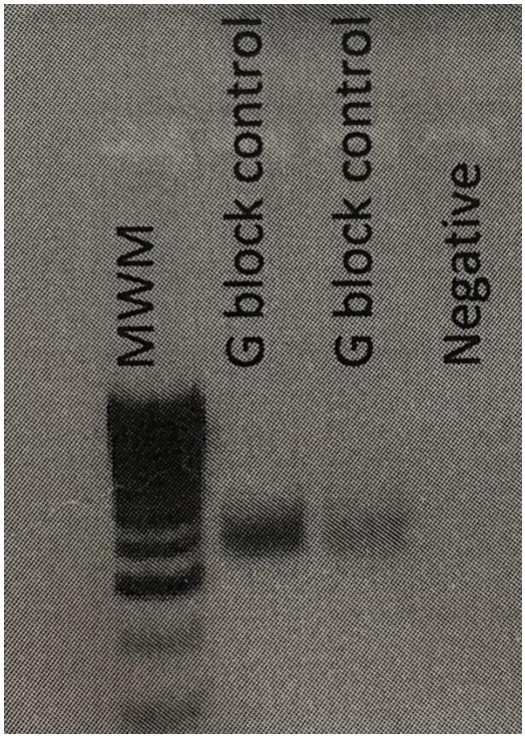

Figure 3.8: Ethidium bromide-stained gel showing the *BRAF-KIAA1549* fusion PCR product. The product size is 228 or 402 base pairs depending on the fusion present.

MWM: Molecular Weight Marker

G-block control: Positive control is *BRAF-KIAA1549* gene fragment (G-block)

Negative: Negative control

Chapter 4

Discussion

The most frequent type of brain tumour identified in children under the age of 20 is PA. [23] They are circumscribed astrocytic gliomas associated with a favourable overall survival and thus regarded as low grade by the World Health Organisation (WHO). [2,3] Complete surgical resection is curative; however, their clinical course can be unfavourable and associated with morbidity. In our research, we discovered a correlation of statistical significance between the risk of recurrence in PAs and certain demographic characteristics. Advances in molecular research on the implications of specific genetic aberrations on tumour relapses have been conflicting. The current series proposed that *BRAF* gene mutations do not add prognostic or diagnostic value in PAs.

Approximately 200 children should present annually in South Africa with PAs, substantiated by updated population estimates from Statistics South Africa 2022 for children under the age of 19. We report a statistically higher incidence from 2000 to 2009 (50.72%). Our data was limited to RCCH, excluding cases from other paediatric neuro-oncology centres. As a result, it was impossible to calculate the overall incidence or prevalence of PAs with any degree of accuracy.

Harmouch et al. [75] and Malik et al. [76] reported a mean age of 8.36 and 10.6 years, which is slightly older than the six years of age we found. Published data reveal a tendency of no sex predilection or a slight male predominance, which contrasts with our findings of a 1: 1.57 male-to-female ratio. [3,77] Due to insufficient clinical data, we could not determine the gender in 15 cases.

PAs can develop anywhere along the neuroaxis. However, they seem to favour the posterior fossa, 40 to 50% present in the cerebellum. [3,78] This is supported by our investigation, which found a predominance of cerebellar tumours in (62%), followed by the cerebral hemisphere (19%), diencephalon (9%) and optic chiasm (6%). Cerebellar tumours appeared in 100% of children under the age of 1 year compared to an equal distribution between cerebral hemispheres (45.45%) and cerebellar tumours (45.45%) in the 11 to 15-year age group. We believe selection bias may have contributed to the anatomic distribution given the young patient population (4 months to 13 years). It is well known that PAs presenting in the cerebral hemisphere are more common in adults. [3]

Histological findings were similar in all cases displaying the characteristic biphasic nature of PAs. The more loosely textured microcystic regions contrasted with the compact piloid zones. None of the patients showed worrisome microscopic features, including those with recurrent tumours.

Our results showed that PA recurrence was significantly correlated with the anatomic site. Tumour relapse or progression was confirmed on radiological and histomorphological findings in 20 patients. Interestingly, 8 (62%) out of 13 cerebral tumours recurred. This contrasts with the low frequency (8 out of 43) of relapses in cerebellar PAs. The association of tumour recurrence and supratentorial anatomic location were statistically significant (p= 0.006). These findings correlate with reports of a better outcome in cerebellar tumours than in non-cerebellar tumours. [79–81]

Complete surgical resection is the treatment of choice. [78] Twelve of the recurrent tumours had conclusive post-operative evidence of surgical removal. Tumour debulking with subsequent partial resection led to recurrence in 6 patients. Thus, frequent recurrence and associated sequelae are worrisome. Burkhard et al. [3] reported 88% and 50% survival rates at 5 and 10 years, respectively, even in the setting of proven postoperative residual tumours. There were no deaths reported in this research.

Exploration of molecular biomarkers to improve patient outcome, especially in partially resected PAs, have been undertaken; however, the findings are contradictory. Essentially all PAs have deregulation of the MAPK signalling pathway with genetic alterations frequently involving the *BRAF* gene. *BRAF-KIAA1549* gene fusion (60-75%) is the most common, followed by *BRAF V600E* mutations (9%). [53,60] Some scientific studies found that the *BRAF-KIAA1549* gene rearrangement is associated with favourable outcomes. [6,7] However, others could not confirm this. [82] *BRAF V600E* mutations are often reported in adults and supratentorial tumours. [14]

This cohort focused on identifying *BRAF* genetic alterations by assessing gene rearrangements and mutations. Immunohistochemistry using the anti-*BRAF V600E* (VE1) antibody is a valuable surrogate for detecting *BRAF V600E* mutations. IHC was successfully performed in all cases, using papillary thyroid carcinoma as a positive control and internal controls as negative. None of the patients showed mutant-BRAF staining. Limitations of staining include tissue ischemia, suboptimal tissue fixation conditions and insufficient tissue samples. [83]

Faulkner et al. [60] suggested that *BRAF* gene rearrangements could serve as a biomarker for diagnosis and prognosis in PAs. In this study, FISH was successfully performed in 30 cases, and none had a re-arrangement at chromosome 7q34 encompassing the *BRAF* gene. Technical problems are often encountered when performing FISH analysis, including the age of the case, small sample size with a scarcity of tumour cells and inadequate tissue fixation resulting in DNA damage.

We proceeded with RT-PCR to detect *BRAF-KIAA1549* fusion transcripts with cDNA from FFPE tissue. RNA was extracted from 32 samples and extraction control. The spectrophotometer readings showed a yield of between 1.10-436.10ng/ul. The absorbance ratio at 260nm (A260) and 280nm (A280) was used to assess the purity of RNA. A ratio of 2.0 is generally regarded as "pure" for RNA. Our cohort's A 260/280 ratio ranged from 1.20 to 2.04. Contamination by, for instance, organic compounds might explain the lower ratio reported in certain samples. This did, however, not affect cDNA synthesis and the RNA in these samples was of appropriate quality.

The extreme sensitivity of RT-PCR makes it susceptible to contamination. Thus, the amplification process's performance depends on the RNA's quality as starting material. [84] To verify the accurate detection of contamination and acceptable RNA quality, we ran a positive and negative control sample, a housekeeping gene, and the case of interest. The positive control comprised targeted synthetic oligonucleotides, G-block Gene Fragments specific for BRAF-KIAA1549 fusion, and it showed amplification with PCR. Beta actin was used as a housekeeping gene, and its presence was confirmed in all cases subjected to PCR testing. We report no contamination of any of the negative controls. In our series, no sample exhibited the *BRAF-KIAA1549* gene fusion. Unfortunately, one of the significant limitations of RT-PCR is its inability to detect different combinations of *BRAF-KIAA1549* exons and other fusion partners. [85] Fifty-four cases were excluded due to poor fixation, poor RNA quality and scarcity of tissue.

Study limitations:

The data we presented in the current series did have limitations. Convenient sampling was done due to the retrospective nature of this series. Other factors included a lack of patient follow-up, deficient clinical information, scarcity of preserved tissue and cases older than 20 years.

The PCR analysis used for *BRAF-KIAA1549* fusion transcripts was limited to detecting fusions involving exon 16 and 11 of the *KIAA1549* and *BRAF* gene, respectively. Fusions involving other exons or other fusion partners were not detected. The quality of the RNA, poor fixation, scarcity of tissue and negative Beta actin resulted in cases being excluded from the current series.

Chapter 5

Conclusion and Recommendation

In conclusion, our findings differ from published literature regarding the younger age of patient presentation, female predominance, and higher frequency of cerebellar tumours. We were unable to address the hypothesis since no *BRAF* genetic alterations were found. Despite substantial advancements in our knowledge of the pathogenesis of PAs, there needs to be more evidence regarding how molecular biomarkers affect clinicopathological traits. We advise prospective research studies to investigate further the effect of genetic aberrations on clinicopathological findings and tumour recurrence rates. We hope these will provide definite diagnostic and therapeutic biomarkers in PAs to decrease the risk of recurrence and morbidity associated with treatment.

References

1. Collins V, Jones D, Giannini C. Pilocytic astrocytoma: pathology, molecular mechanisms and markers. *Acta Neuropathol*. 2015;129. doi:10.1007/s00401-015-1410-7
2. Stüer C, Vilz B, Majores M, Becker A, Schramm J, Simon M. Frequent recurrence and progression in pilocytic astrocytoma in adults. *Cancer Interdiscip Int J Am Cancer Soc*. 2007;110(12):2799-2808.
3. Burkhard C, Di Patre P-L, Schüler D, et al. A population-based study of the incidence and survival rates in patients with pilocytic astrocytoma. *J Neurosurg*. 2003;98(6):1170-1174.
4. Louis DN. *WHO Classification of Tumours of the Central Nervous System*. 5th editio. IARC; 2021.
5. Maraka S, Janku F. BRAF alterations in primary brain tumors. *Discov Med*. 2018;26(141):51-60.
6. Hawkins C, Walker E, Mohamed N, et al. BRAF-KIAA1549 fusion predicts better clinical outcome in pediatric low-grade astrocytoma. *Clin Cancer Res*. 2011;17(14):4790-4798.
7. Horbinski C, Hamilton RL, Nikiforov Y, Pollack IF. Association of molecular alterations, including BRAF, with biology and outcome in pilocytic astrocytomas. *Acta Neuropathol*. 2010;119(5):641-649.
8. Jones DTW, Kocialkowski S, Liu L, et al. Tandem duplication producing a novel oncogenic BRAF fusion gene defines the majority of pilocytic astrocytomas. *Cancer Res*. 2008;68(21):8673-8677.
9. Steliarova-Foucher E, Colombet M, Ries LAG, et al. International incidence of childhood cancer, 2001–10: a population-based registry study. *Lancet Oncol*. 2017;18(6):719-731.
10. Wallner KE, Gonzales MF, Edwards MSB, Wara WM, Sheline GE. Treatment results of juvenile pilocytic astrocytoma. *J Neurosurg*. 1988;69(2):171-176.
11. Abdollahzadeh M, Hoffman HJ, Blazer SI, et al. Benign cerebellar astrocytoma in childhood: experience at the Hospital for Sick Children 1980–1992. *Child's Nerv Syst*. 1994;10(6):380-383.
12. Bartek J, Dhawan S, Thurin E, et al. Short-term outcome following surgery for rare brain tumor entities in adults: a Swedish nation-wide registry-based study and comparison with SEER database. *J Neurooncol*. 2020;148(2):281-290.
13. Clark GB, Henry JM, McKeever PE. Cerebral pilocytic astrocytoma. *Cancer*.

1985;56(5):1128-1133.
14. Lapointe S, Perry A, Butowski NA. Primary brain tumours in adults. *Lancet*. 2018;392(10145):432-446.
15. Koeller KK, Rushing EJ. From the archives of the AFIP: pilocytic astrocytoma: radiologic-pathologic correlation. *Radiographics*. 2004;24(6):1693-1708.
16. Gol A, McKissock W. The cerebellar astrocytomas: a report on 98 verified cases. *J Neurosurg*. 1959;16(3):287-296.
17. Kleihues P, Louis DN, Scheithauer BW, et al. The WHO classification of tumors of the nervous system. *J Neuropathol Exp Neurol*. 2002;61(3):215-225.
18. Pandit B, Sarkozy A, Pennacchio LA, et al. Gain-of-function RAF1 mutations cause Noonan and LEOPARD syndromes with hypertrophic cardiomyopathy. *Nat Genet*. 2007;39(8):1007-1012.
19. Niihori T, Aoki Y, Narumi Y, et al. Germline KRAS and BRAF mutations in cardio-facio-cutaneous syndrome. *Nat Genet*. 2006;38(3):294-296.
20. Listernick R, Louis DN, Packer RJ, Gutmann DH. Optic pathway gliomas in children with neurofibromatosis 1: consensus statement from the NF1 Optic Pathway Glioma Task Force. *Ann Neurol Off J Am Neurol Assoc Child Neurol Soc*. 1997;41(2):143-149.
21. Jones DTW, Gronych J, Lichter P, Witt O, Pfister SM. MAPK pathway activation in pilocytic astrocytoma. *Cell Mol Life Sci*. 2012;69(11):1799-1811.
22. Louis DN, Reifenberger G, Brat DJ, Ellison DW. Tumours: introduction and neuroepithelial tumours. *Greenfield's Neuropathol*. 2008;8:1821-2000.
23. Kleihues P, Sobin LH. World Health Organization classification of tumors. *Cancer*. 2000;88(12):2887.
24. Schuettpelz LG, McDonald S, Whitesell K, et al. Pilocytic astrocytoma in a child with Noonan syndrome. *Pediatr Blood Cancer*. 2009;53(6):1147-1149.
25. Miglioretti DL, Johnson E, Williams A, et al. The use of computed tomography in pediatrics and the associated radiation exposure and estimated cancer risk. *JAMA Pediatr*. 2013;167(8):700-707.
26. Pencalet P, Maixner W, Sainte-Rose C, et al. Benign cerebellar astrocytomas in children. *J Neurosurg*. 1999;90(2):265-273.
27. Collins VP, Jones DTW, Giannini C. Pilocytic astrocytoma: pathology, molecular mechanisms and markers. *Acta Neuropathol*. 2015;129(6):775-788.
28. Minehan KJ, Shaw EG, Scheithauer BW, Davis DL, Onofrio BM. Spinal cord astrocytoma: pathological and treatment considerations. *J Neurosurg*. 1995;83(4):590-595.
29. Borit A, Richardson Jr EP. The biological and clinical behaviour of pilocytic

astrocytomas of the optic pathways. *Brain a J Neurol*. 1982;105(Pt 1):161-187.
30. Grcevic N, Yates PO. Rosenthal fibres in tumours of the central nervous system. *J Pathol Bacteriol*. 1957;73(2):467-472.
31. Seilhean D, De Girolami U, Gray F. Basic pathology of the central nervous system. In: *Escourolle & Poirier Manual of Basic Neuropathology*. Elsevier; 2004:1-20.
32. Lach B, Sikorska M, Rippstein P, Gregor A, Staines W, Davie TR. Immunoelectron microscopy of Rosenthal fibers. *Acta Neuropathol*. 1991;81(5):503-509.
33. Chourmouzi D, Papadopoulou E, Konstantinidis M, et al. Manifestations of pilocytic astrocytoma: a pictorial review. *Insights Imaging*. 2014;5(3):387-402.
34. Hitotsumatsu T, Iwaki T, Fukui M, Tateishi J. Cytoplasmic inclusions of astrocytic elements of glial tumors: special reference to round granulated body and eosinophilic hyaline droplets. *Acta Neuropathol*. 1994;88(6):501-510.
35. Giannini C, Scheithauer BW, Burger PC, et al. Cellular proliferation in pilocytic and diffuse astrocytomas. *J Neuropathol Exp Neurol*. 1999;58(1):46-53.
36. Rodriguez FJ, Scheithauer BW, Burger PC, Jenkins S, Giannini C. Anaplasia in pilocytic astrocytoma predicts aggressive behavior. *Am J Surg Pathol*. 2010;34(2):147-160.
37. Collins VP, Jones DTW, Giannini C. Pilocytic astrocytoma: pathology, molecular mechanisms and markers. *Acta Neuropathol*. 2015;129(6):775-788.
38. Burger PC, Khandji AG, Tihan T, et al. Pilomyxoid astrocytoma: a review. *Medscape Gen Med*. 2004;6(4).
39. Jones DTW, Hutter B, Jäger N, et al. Recurrent somatic alterations of FGFR1 and NTRK2 in pilocytic astrocytoma. *Nat Genet*. 2013;45(8):927-932.
40. Zhang J, Wu G, Miller CP, et al. Whole-genome sequencing identifies genetic alterations in pediatric low-grade gliomas. *Nat Genet*. 2013;45(6):602.
41. Seger R. *MAP Kinase Signaling Protocols*. Vol 250. Springer Science & Business Media; 2004.
42. Zhang W, Liu HT. MAPK signal pathways in the regulation of cell proliferation in mammalian cells. *Cell Res*. 2002;12(1):9-18.
43. Ji R-R, Gereau IV RW, Malcangio M, Strichartz GR. MAP kinase and pain. *Brain Res Rev*. 2009;60(1):135-148.
44. Sweatt JD. The neuronal MAP kinase cascade: a biochemical signal integration system subserving synaptic plasticity and memory. Journal of neurochemistry.
45. Tatevossian RG, Lawson ARJ, Forshew T, Hindley GFL, Ellison DW, Sheer D. MAPK pathway activation and the origins of pediatric low-grade astrocytomas. *J Cell Physiol*. 2010;222(3):509-514.
46. Matallanas D, Birtwistle M, Romano D, et al. Raf family kinases: old dogs have

learned new tricks. *Genes Cancer*. 2011;2(3):232-260.

47. Van Gastel J, Hendrickx JO, Leysen H, et al. β-Arrestin based receptor signaling paradigms: Potential therapeutic targets for complex age-related disorders. *Front Pharmacol*. 2018;9:1369.
48. Khater F, Langlois S, Cassart P, et al. Recurrent somatic BRAF insertion (p. V504_R506dup): a tumor marker and a potential therapeutic target in pilocytic astrocytoma. *Oncogene*. 2019;38(16):2994-3002.
49. Ahn JS, Harrison W, Hughes E, McLendon RE. Intraventricular Pilocytic Astrocytoma With KIAA1549/BRAF Fusion Arising in a 44-Year Old. *J Neuropathol Exp Neurol*. 2019;78(2):187-190.
50. Chen YH, Gutmann DH. The molecular and cell biology of pediatric low-grade gliomas. *Oncogene*. 2014;33(16):2019-2026.
51. Tomić TT, Olausson J, Wilzén A, et al. A new GTF2I-BRAF fusion mediating MAPK pathway activation in pilocytic astrocytoma. *PLoS One*. 2017;12(4):e0175638.
52. Brokinkel B, Brentrup A, Stummer W, et al. Scientific Correspondence. *Neuropathol Appl Neurobiol*. 2015;41(2):258-261.
53. Brokinkel B, Peetz-Dienhart S, Ligges S, et al. A comparative analysis of MAPK pathway hallmark alterations in pilocytic astrocytomas: age-related and mutually exclusive.[corrected]. *Neuropathol Appl Neurobiol*. 2015;41(2):258-261.
54. Yao Z, Torres NM, Tao A, et al. BRAF mutants evade ERK-dependent feedback by different mechanisms that determine their sensitivity to pharmacologic inhibition. *Cancer Cell*. 2015;28(3):370-383.
55. Yao Z, Yaeger R, Rodrik-Outmezguine VS, et al. Tumours with class 3 BRAF mutants are sensitive to the inhibition of activated RAS. *Nature*. 2017;548(7666):234-238.
56. Śmiech M, Leszczyński P, Kono H, Wardell C, Taniguchi H. Emerging BRAF mutations in cancer progression and their possible effects on transcriptional networks. *Genes (Basel)*. 2020;11(11):1342.
57. Bar EE, Lin A, Tihan T, Burger PC, Eberhart CG. Frequent gains at chromosome 7q34 involving BRAF in pilocytic astrocytoma. *J Neuropathol Exp Neurol*. 2008;67(9):878-887. doi:10.1097/NEN.0b013e3181845622
58. Pfister S, Janzarik WG, Remke M, et al. BRAF gene duplication constitutes a mechanism of MAPK pathway activation in low-grade astrocytomas. *J Clin Invest*. 2008;118(5):1739-1749.
59. Tian Y, Rich BE, Vena N, et al. Detection of KIAA1549-BRAF fusion transcripts in formalin-fixed paraffin-embedded pediatric low-grade gliomas. *J Mol Diagnostics*. 2011;13(6):669-677.
60. Faulkner C, Ellis HP, Shaw A, et al. BRAF fusion analysis in pilocytic astrocytomas:

KIAA1549-BRAF 15-9 fusions are more frequent in the midline than within the cerebellum. *J Neuropathol Exp Neurol*. 2015;74(9):867-872.

61. Schindler G, Capper D, Meyer J, et al. Analysis of BRAF V600E mutation in 1,320 nervous system tumors reveals high mutation frequencies in pleomorphic xanthoastrocytoma, ganglioglioma and extra-cerebellar pilocytic astrocytoma. *Acta Neuropathol*. 2011;121(3):397-405.
62. Steinbok P, Poskitt K, Hendson G. Spontaneous regression of cerebellar astrocytoma after subtotal resection. *Child's Nerv Syst*. 2006;22(6):572-576.
63. Due-Tønnessen BJ, Lundar T, Egge A, Scheie D. Neurosurgical treatment of low-grade cerebellar astrocytoma in children and adolescents: a single consecutive institutional series of 100 patients. *J Neurosurg Pediatr*. 2013;11(3):245-249.
64. Parsons MW, Whipple NS, Poppe MM, Mendez JS, Cannon DM, Burt LM. The use and efficacy of chemotherapy and radiotherapy in children and adults with pilocytic astrocytoma. *J Neurooncol*. 2021;151(2):93-101.
65. Sutton LN, Cnaan A, Klatt L, et al. Postoperative surveillance imaging in children with cerebellar astrocytomas. *J Neurosurg*. 1996;84(5):721-725.
66. Vassilyadi M, Shamji MF, Tataryn Z, Keene D, Ventureyra E. Postoperative surveillance magnetic resonance imaging for cerebellar astrocytoma. *Can J Neurol Sci*. 2009;36(6):707-712.
67. Krishnatry R, Zhukova N, Guerreiro Stucklin AS, et al. Clinical and treatment factors determining long-term outcomes for adult survivors of childhood low-grade glioma: a population-based study. *Cancer*. 2016;122(8):1261-1269.
68. Campbell JW, Pollack IF. Cerebellar astrocytomas in children. *J Neurooncol*. 1996;28(2-3):223-231. doi:10.1007/BF00250201
69. Lawrence YR, Li XA, El Naqa I, et al. Radiation dose–volume effects in the brain. *Int J Radiat Oncol Biol Phys*. 2010;76(3):S20-S27.
70. Merchant TE, Conklin HM, Wu S, Lustig RH, Xiong X. Late effects of conformal radiation therapy for pediatric patients with low-grade glioma: prospective evaluation of cognitive, endocrine, and hearing deficits. *J Clin Oncol*. 2009;27(22):3691.
71. Bowers DC, Liu Y, Leisenring W, et al. Late-occurring stroke among long-term survivors of childhood leukemia and brain tumors: a report from the Childhood Cancer Survivor Study. *J Clin Oncol*. 2006;24(33):5277-5282.
72. Dankner M, Rose AAN, Rajkumar S, Siegel PM, Watson IR. Classifying BRAF alterations in cancer: new rational therapeutic strategies for actionable mutations. *Oncogene*. 2018;37(24):3183-3199.
73. Horbinski C, Nikiforova MN, Hagenkord JM, Hamilton RL, Pollack IF. Interplay among BRAF, p16, p53, and MIB1 in pediatric low-grade gliomas. *Neuro Oncol*.

2012;14(6):777-789.

74. Cin H, Meyer C, Herr R, et al. Oncogenic FAM131B–BRAF fusion resulting from 7q34 deletion comprises an alternative mechanism of MAPK pathway activation in pilocytic astrocytoma. *Acta Neuropathol*. 2011;121(6):763-774.
75. Harmouch A, Taleb M, Lasseini A, Maher M, Sefiani S. Epidemiology of pediatric primary tumors of the nervous system: a retrospective study of 633 cases from a single Moroccan institution. *Neurochirurgie*. 2012;58(1):14-18.
76. Malik A, Deb P, Sharma MC, Sarkar C. Neuropathological spectrum of pilocytic astrocytoma-an Indian series of 120 cases. *Pathol Oncol Res*. 2006;12:164-171.
77. Burger PC, Scheithauer BW, Paulus W, Szymas J, Giannini C, Kleihues P. Pathology and genetics of tumours of the nervous system. *Lyon IARC*. Published online 2000:45-51.
78. Khan MA, Godil SS, Tabani H, Panju SA, Enam SA. Clinical review of pediatric pilocytic astrocytomas treated at a tertiary care hospital in Pakistan. *Surg Neurol Int*. 2012;3.
79. Colin C, Padovani L, Chappe C, et al. Outcome analysis of childhood pilocytic astrocytomas: a retrospective study of 148 cases at a single institution. *Neuropathol Appl Neurobiol*. 2013;39(6):693-705.
80. Zakrzewski K, Jarząb M, Pfeifer A, et al. Transcriptional profiles of pilocytic astrocytoma are related to their three different locations, but not to radiological tumor features. *BMC Cancer*. 2015;15:1-16.
81. Fernandez C, Figarella-Branger D, Girard N, et al. Pilocytic astrocytomas in children: Prognostic factors - A retrospective study of 80 cases. *Neurosurgery*. 2003;53(3):544-555. doi:10.1227/01.NEU.0000079330.01541.6E
82. Terashima K, Chow K, Jones J, et al. Long-term outcome of centrally located low-grade glioma in children. *Cancer*. 2013;119(14):2630-2638.
83. Taylor CR, Levenson RM. Quantification of immunohistochemistry—issues concerning methods, utility and semiquantitative assessment II. *Histopathology*. 2006;49(4):411-424.
84. Weiss SW, Goldblum JR, Folpe AL. *Enzinger and Weiss's Soft Tissue Tumors*. Elsevier Health Sciences; 2007.
85. Appay R, Fina F, Macagno N, et al. Duplications of KIAA1549 and BRAF screening by Droplet Digital PCR from formalin-fixed paraffin-embedded DNA is an accurate alternative for KIAA1549-BRAF fusion detection in pilocytic astrocytomas. *Mod Pathol*. 2018;31(10):1490-1501.

Appendix 1 – Ethics approval

HUMAN RESEARCH ETHICS COMMITTEE
13 JUL 2023
HEALTH SCIENCES FACULTY
UNIVERSITY OF CAPE TOWN

UNIVERSITY OF CAPE TOWN
IYUNIVESITHI YASEKAPA • UNIVERSITEIT VAN KAAPSTAD

FACULTY OF HEALTH SCIENCES
Human Research Ethics Committee

FHS016: Annual Progress Report / Renewal

HREC office use only (FWA00001637; IRB00001938) This serves as notification of annual approval, including any documentation described below.			
☑ Approved	Annual progress report	Approved until/next renewal date	30/7/2024
☐ Not approved	See attached comments		
Signature Chairperson of the HREC/ Designee	Signed by candidate	Date Signed	13/7/2023

Note: Please email this form and supporting documents (if applicable) in a combined pdf-file to hrec-enquiries@uct.ac.za.
Please clarify your plan for research-related activities during COVID-19 lockdown.
Please use the latest form found on our website:
http://www.health.uct.ac.za/fhs/research/humanethics/forms

Comments to PI from the HREC

Principal Investigator to complete the following:

1. Protocol information

Date (when submitting this form)	10 July 2023		
HREC REF Number	440/2021	Current Ethics Approval was granted until	30 July 2023
Protocol title	The relationship between V-raf murine sarcoma viral oncogene homolog B1 (BRAF) genetic alterations and the risk of tumour recurrence in pilocytic astrocytomas in children diagnosed at Red Cross Children's Hospital over a 30-year period.		
Protocol number (if applicable)			
Are there any sub-studies linked to this study?	☐ Yes	☐ ✓No	
If yes, could you please provide the HREC Reference number for all sub-studies? **Note:** A separate FHS016 must be submitted for each sub-study.			

(Note: Please complete the Closure form (FHS010) if the study is completed within the approval period)

Appendix 2 – Preparation of reagents

Nucleotide sequence of the gBlocks® Gene Fragment - 501-750 bp

BRAF-KIAA1549

CCGGCGTCCACAACTCAGCCTACATCGGATGCCCATCGGATCCTGACCTCCCAGCCGA
TGTGCAGACACCATCCTCGGTGGAACTGGGGAGGTATCCAGCCCTTCCCTTCCCGGCC
TCCCAGTACATCCCACCCCAGCCGTCCATCGAGGAGGCACGCCAGACCATGCACTCC
CTCCTGGACGACGCCTTTGCCCTCGTGGCCCCCAGCAGCCAGCCTGCCAGCACCGCA
GGTGTAGGCCCCGGAGTCCCACCCGGCCTGCCCGCAAACAGCACCCCTTCCCAGGAA
GAGAGGCGAGCCACCCAGTGGGGGTCCTTCTACAGCCCAGCCCAGACGGCCAACAAT
CCCTGCAGTGACTTGATTAGAGACCAAGGATTTCGTGGTGATGGAGGATCAACCACAG
GTTTGTCTGCTACCCCCCCTGCCTCATTACCTGGCTCACTAACTAACGTGAAAGCCTTA
CAGAAATCTCCAGGACCTCAGCGAGAAAGGAAGTCATCTTCATCCTCAGAAGACAGGA
ATCGAATGAAAACACTTGGTAGACGGGACTCGAGTGAT

The sequence in bold and underline shows the position of the forward and reverse primers.

Immunohistochemistry

1. Three-micron tissue sections were cut from formalin-fixed paraffin-embedded and picked up onto Histobond slides.
2. The slides were incubated overnight at 60°C
3. Sections were deparaffinised in xylene, rehydrated in graded ethanol and washed in water.
4. Endogenous peroxidase activity was blocked by treating the slides with a 3% hydrogen peroxide (H2O2) solution for 10 minutes.
5. The slides were washed well in water.
6. After washing, heat-mediated antigen retrieval was performed using EDTA
7. Slides were then rinsed in PBS
8. Slides were then blocked for non-specific binding using a 5% goat serum solution at room temperature for 10 minutes (DAKO: X0907)

9. The goat serum was drained off, and the slides were incubated with the primary antibodies for 45 minutes at room temperature.
10. After incubation, the slides were washed in PBS.
11. Slides were then treated with goat antimouse immunoglobulins labelled with horse radish peroxidase (DAKO: Envision K4001) at room temperature for 30 minutes.
12. The slides were then washed well in PBS.
13. Positivity was developed by applying 3.3 diaminobenzidine (DAKO: K3466) at room temperature for 5-10 minutes.
14. Slides were washed well in water
15. Slides were then immersed in a 1% $CuSO_4$ solution for 5 minutes
16. Slides were then rinsed well in running water
17. Slides were counterstained in haematoxylin for 30 seconds and blued in Scott's tap water.
18. Slides were washed in water, followed by dehydration using graded ethanols, cleared with xylene then mounted with Entallan.

Fluorescence in-situ hybridisation

1. 20xSSC (3M sodium chloride; 0.3M sodium citrate), pH 5.3
   66g of 20xSSC was added to 200ml of sterile H_2O. These components were mixed well, followed by a pH adjustment to 5.3 with 1N HCl. The solution was topped with sterile water to a final volume of 250ml and stored at room temperature (RT) for six months.
2. Post-hybridisation wash buffer (2xSSC/0.3% IGEPAL CA-630)
   50ml of 20XSSC (pH 5.3) was added to 420ml of sterile H2O. This was mixed thoroughly, and the pH was adjusted to 7.25 with 1N NaOH. Subsequently, 1.5ml of IGEPAL CA-630 was added by gently pipetting the viscous solution and allowed to mix well. The mixture was topped up to 500ml with sterile H2O, filtered and stored at RT for six months.
3. 70% (v/v) Ethanol:
   350ml of absolute ethanol was added to 150ml sterile H2O.
4. 85% (v/v) Ethanol:
   425ml of absolute ethanol was added to 75ml sterile H2O.
5. 0.2N HCl:
   5ml concentrated HCl (32% = 10.4N) was added to 245ml sterile H2O.
6. 0.01N HCl:
   1.5ml 0.2N HCl was added to 28.5ml sterile H2O.
7. 10% pepsin (w/v):

500mg pepsin was added to 5ml sterile H_2O. Aliquots of 80µl were made in 0.2ml tubes and placed in a freezer.

8. Pepsin working solution:
   75µl of 10% pepsin was added to 30ml 0.01N HCl.
9. 1M Sodium thiocyanate buffer:
   20.3g of sodium thiocyanate was added to 200 ml of sterile H_2O. This was mixed and topped up to 250ml.

Agarose gel electrophoresis

1. 20xSB Buffer (stock):
   38.14g of disodium tetraborate decahydrate was added to 800 ml of sterile water. This was mixed, topped to a final volume of 1000ml with sterile water and stored at room temperature (RT).
2. 1xSB Buffer (working solution):
   50ml of 20xSB Buffer was added to 950ml sterile water and stored at RT.
3. Preparation and casting of 1.5% agarose gel:
   1.5g agarose powder and 100 ml 1xSB buffer were combined in a suitable container (600 ml Erlenmeyer flask or beaker). The flask was placed in a microwave oven and boiled for 2 minutes. After that, the molten agarose cooled for 5-7 minutes before 3µl of ethidium bromide was added. The gel was poured into an assembled casting tray when it was cool enough. The appropriate combs were inserted, and the gel was set for at least 30 minutes.

Appendix 3 – Composite table of data captured and generated during this study

Case:	Site:	Age:	Gender	Treatment received	Recurrence	BRAF IHC	BRAF FISH
1	Cerebral hemisphere	9	Male	Surgery: resection	Recurrence	Negative	No rearrangement
2	Cerebellum	10	Female	Surgery: resection	No recurrence	Negative	No rearrangement
3	Cerebellum	2	Female	Surgery: resection	No recurrence	Negative	No rearrangement
4	Cerebellum	2	Female	Surgery: resection	No recurrence	Negative	Tissue insufficient
5	Diencephalon	7	Male	Surgery: debulking	No recurrence	Negative	No rearrangement
6	Optic tract	5	No data	No data available	No recurrence	Negative	No rearrangement
7	Diencephalon	6	Male	Surgery: resection	No recurrence	Negative	Tissue insufficient
8	Optic tract	6	No data	No data available	No recurrence	Negative	Tissue insufficient
9	Cerebellum	7	Male	Surgery: resection	No recurrence	Negative	No rearrangement
10	Cerebellum	12	Female	Surgery: resection	Recurrence	Negative	Tissue insufficient
11	Cerebellum	6	Female	No surgery (chemotherapy and radiation)	No recurrence	Negative	Tissue insufficient
12	Cerebellum	8	Male	Surgery: resection	Recurrence	Negative	Tissue insufficient
13	Cerebellum	4 months	Male	No surgery (chemotherapy and radiation)	No recurrence	Negative	Tissue insufficient
14	Cerebellum	7	No data	No data available	No recurrence	Negative	No rearrangement
15	No data available	No data available	No data	No data available	Recurrence	Negative	No rearrangement
16	Diencephalon	7	Male	Surgery: resection	Recurrence	Negative	Tissue insufficient
17	Cerebellum	5	Female	Surgery: resection	Recurrence	Negative	No rearrangement
18	Cerebellum	3	No data	No data available	No recurrence	Negative	No rearrangement
19	Cerebellum	12	Female	Surgery: resection	No recurrence	Negative	No rearrangement
20	Cerebral hemisphere	1	Male	Surgery: resection	Recurrence	Negative	Tissue insufficient
21	Cerebellum	1	Female	Surgery: resection	No recurrence	Negative	Tissue insufficient
22	Cerebellum	7	No data	No data available	No recurrence	Negative	No rearrangement
23	Cerebellum	4	Female	No data available	No recurrence	Negative	No rearrangement
24	Cerebellum	6	Female	Surgery: debulking	Recurrence	Negative	Tissue insufficient
25	Cerebral hemisphere	13	No data	No data available	Recurrence	Negative	No rearrangement
26	Cerebellum	8	No data	No data available	No recurrence	Negative	Tissue insufficient

27	Cerebellum	8	No data	No data available	No recurrence	Negative	No rearrangement
28	Cerebellum	3	No data	No data available	No recurrence	Negative	Tissue insufficient
29	Optic tract	7	No data	No data available	No recurrence	Negative	No rearrangement
30	Cerebral hemisphere	12	No data	No data available	Recurrence	Negative	Tissue insufficient
31	Diencephalon	11	Female	Surgery: resection	No recurrence	Negative	Tissue insufficient
32	Cerebellum	5	Female	Surgery: resection	No recurrence	Negative	Tissue insufficient
33	Cerebral hemisphere	7	Male	No data available	No recurrence	Negative	Tissue insufficient
34	Cerebellum	5	Female	Surgery: resection	No recurrence	Negative	Tissue insufficient
35	Cerebellum	6	Female	No surgery (chemotherapy and radiation)	No recurrence	Negative	Tissue insufficient
36	Cerebral hemisphere	9	Male	Surgery: resection	Recurrence	Negative	Tissue insufficient
37	No data available	No data available	No data	No data available	No data available	Negative	Tissue insufficient
38	Cerebellum	3	Female	Surgery: resection	Recurrence	Negative	Tissue insufficient
39	Cerebellum	10	No data	No data available	No recurrence	Negative	Tissue insufficient
40	Cerebral hemisphere	11	Male	Surgery: resection	No recurrence	Negative	No rearrangement
41	Cerebellum	9	Female	Surgery: resection	No recurrence	Negative	No rearrangement
42	Cerebellum	9	Male	No data available	No recurrence	Negative	No rearrangement
43	Cerebral hemisphere	11	Female	No data available	No recurrence	Negative	No rearrangement
44	Cerebellum	11	No data	No data available	No recurrence	Negative	Tissue insufficient
45	Cerebellum	5	Male	Surgery: resection	No recurrence	Negative	Tissue insufficient
46	Cerebellum	2	Male	Surgery: resection	No recurrence	Negative	No rearrangement
47	Cerebellum	4	Female	Surgery: resection	No recurrence	Negative	No rearrangement
48	Optic tract	2	Male	Surgery: debulking	Recurrence	Negative	Tissue insufficient
49	Cerebellum	3	Male	Surgery: resection	No recurrence	Negative	Tissue insufficient
50	Cerebellum	1	No data	No data available	No recurrence	Negative	Tissue insufficient
51	Cerebellum	2	Female	Surgery: debulking	Recurrence	Negative	No rearrangement
52	Cerebellum	11	Male	Surgery: resection	No recurrence	Negative	No rearrangement
53	Cerebellum	3	Male	Surgery: resection	Recurrence	Negative	No rearrangement
54	Cerebellum	6	Female	Surgery: resection	No recurrence	Negative	Tissue insufficient
55	Diencephalon	6	Male	No data available	No recurrence	Negative	Tissue insufficient
56	Cerebral hemisphere	7	Male	Surgery: resection	Recurrence	Negative	Tissue insufficient
57	Cerebral hemisphere	1	Male	Surgery: resection	Recurrence	Negative	No rearrangement

58	Cerebral hemisphere	10	Female	Surgery: resection	No recurrence	Negative	No rearrangement
59	Cerebellum	13	No data	No data available	No recurrence	Negative	Tissue insufficient
60	Cerebellum	4	Female	Surgery: resection	No recurrence	Negative	Tissue insufficient
61	Cerebral hemisphere	1	Female	Surgery: resection	Recurrence	Negative	No rearrangement
62	Cerebellum	3	Female	Surgery: debulking	No recurrence	Negative	No rearrangement
63	Cerebellum	1	Female	Surgery: resection	Recurrence	Negative	No rearrangement
64	Diencephalon	3	Male	No surgery (chemotherapy and radiation)	Recurrence	Negative	Tissue insufficient
65	Cerebral hemisphere	13	Female	No surgery (chemotherapy and radiation)	No recurrence	Negative	Tissue insufficient
66	Cerebellum	10	Female	No data available	No recurrence	Negative	Tissue insufficient
67	No data available	No data available	No data	No data available	No recurrence	Negative	No rearrangement
68	Cerebellum	8	Female	Surgery: resection	No recurrence	Negative	Tissue insufficient
69	Cerebellum	3	Female	Surgery: resection	No recurrence	Negative	Tissue insufficient

Appendix 4 – Quantity and purity of each case from which RNA was extracted.

Table 1

Sample	RNA (ng/ul)	A260/A280	Beta Actin	*KIAA1549-BRAF*
Blank	0.0	0.2		
1	8,20	1,70	Negative	-
2	55,00	1,90	Negative	-
3	4,00	2,04	Negative	-
4	-	-	-	-
5	17,10	1,20	Positive	Negative
6	17,30	1,89	Positive	Negative
7	-	-	-	-
8	-	-	-	-
9	1,10	1,70	Negative	-
10	21,30	1,24	Negative	-
11	-	-	-	-
12	-	-	-	-
13	-	-	-	-
14	8,40	1,64	Negative	-
15	30,00	1,99	Positive	Negative
16	-	-	-	-
17	24,90	1,75	Positive	Negative
18	-	-	-	-
19	-	-	-	-
20	-	-	-	-
21	26,20	1,62	Positive	Negative
22	61,00	1,95	Negative	-
23	-	-	-	-
24	-	-	-	-
25	-	-	-	-
26	1,90	1,80	Negative	-
27	8,20	1,62	Negative	-
28	9,70	1,88	Positive	Negative
29	-	-	-	-
30	27,70	1,69	Negative	-
31	-	-	-	-
32	23,10	2,02	Negative	-
33	-	-	-	-

34	21,20	1,61	Negative	-
35	11,00	1,92	Negative	-
36	-	-	-	-
37	-	-	-	-
38	-	-	-	-
39	-	-	-	-
40	-	-	-	-
41	17,40	1,97	Positive	Negative
42	15,30	1,82	Positive	Negative
43	-	-	-	-
44	-	-	-	-
45	-	-	-	-
46	18,10	1,90	Positive	Negative
47	22,70	2,05	Positive	Negative
48	5,90	1,42	Negative	-
49	-	-	-	-
50	-	-	-	-
51	435,10	1,46	Positive	Negative
52	15,00	1,94	Negative	-
53	-	-	-	Negative
54	-	-	-	-
55	-	-	-	-
56	-	-	-	Negative
57	29,50	1,87	Negative	-
58	13,30	1,76	Negative	-
59	-	-	-	-
60	-	-	-	-
61	-	-	-	Negative
62	44,90	1,87	Negative	-
63	44,90	1,87	Negative	-
64	-	-	-	-
65	-	-	-	-
66	-	-	-	-
67	40,30	1,72	Negative	-
68	42,30	1,86	Positive	Negative
69	-	-	-	-